This project has received funding from the European Union's Seventh Programme for research, technological development and demonstration under grant agreement No [308417]".

New Directions in Seismic Hazard Assessment through Focused Earth Observation in the Marmara Supersite

Grant Agreement Number: 308417 co-funded by the European Commission within the Seventh Framework Programme
THEME [ENV.2012.6.4-2] [Long-term monitoring experiment in geologically active regions of Europe prone to natural hazards: the Supersite concept]

D7.3

Report on the integration of faulting parameters from palaeoseismic and historical data for hazard assessment

Project Start Date	1 November 2012
Project Duration	42 Months
Project Coordinator /Organization	Nurcan Meral Özel / KOERI
Work Package Number	WP 7
Deliverable Name/ Number	Report on the integration of faulting parameters from palaeoseismic and historical data for hazard assessment /D 7.3
Due Date Of Deliverable	30 April 2016
Actual Submission Date	2 May 2016
Organization/Author (s)	CNR-ISMAR / Luca Gasperini, INGV / Stefano Pucci, Simone Orefice, Riccardo Civico, Paolo Marco De Martini, Francesca Romana Cinti, Alessandra Smedile, Daniela Pantosti. ITU / K. Kadir Eriş, M. Namık Çağatay, Burak Yalamaz, Nurettin Yakupoğlu, Cengiz Zabcı

Dissemination Level		
PU	Public	
PP	Restricted to other programme participants (including the Commission)	
RE	Restricted to a group specified by the consortium (including the Commission)	
CO	Confidential, only for members of the consortium (including the Commission)	

Table of Contents

The Morphostructural map of the Sea of Marmara

Based on a new morphostructural map (Figure 1), compiled using all available high-resolution seismic reflection profiles and multibeam data collected during MARMARA2013 expedition (Gasperini et al., 2013), we propose a seismic hazard scenario for the active fault segments, which constitute the so called Main Marmara Fault (Le Pichon et al., 2001). This long and deep seated feature is considered the most important seismogenic structure in the Sea of Marmara, along the principal deformation zone of the North Anatolian Fault.

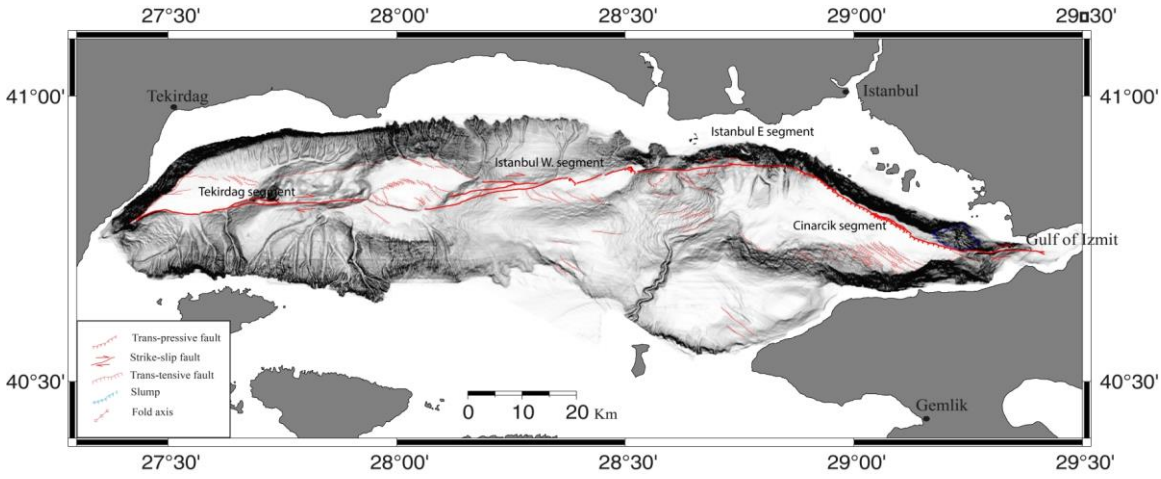

Figure 1 A new morphostructural map of the Marmara Main Fault (Le Pichon et al., 2001) based on the data collected during MARMARA2013 expedition (Gasperini et al., 2013).

The newly compiled map highlights the presence of several individual segments, whose morphometrical and structural analyses enabled us to estimate a maximum expected magnitude during major earthquakes using empirical laws (Wells and Coppersmith, 1994).

Our analysis was carried out considering fault activity at the scale of the Holocene (10 ka), because this stratigraphic level is marked in the Sea of Marmara by a

characteristic unconformity (Cagatay et al., 2001; Polonia et al., 2004). Moreover, giving the fact that the average recurrence time of large magnitude earthquake over a single segment of the NAF is around 250-300 years (Ambrasays and Finkel, xxx) a time span of 10 ka should include several earthquake cycles, being representative of the structural behavior of the fault at geological time intervals.

We observed 3 styles of active deformation in the Sea of Marmara: 1) almost pure strike-slip, oriented E-W; 2) trans-tensional, NE-SW oriented, which is the most common pattern; trans-pressive, forming structures oriented NW-SE. At the scale of the entire Sea of Marmara, 3/4 major segments were recognized (Figure 1). From E to W, they were called: the *Cinarcik Segment*, located to the E of Istanbul; *the Istanbul East*, and *West segments,* located parallel to the coast in front of Istanbul; the *Tekirdag Segment,* from the Central Basin to the western coast of the Sea of Marmara, where the Main Marmara Fault connects with the Ganos Fault.

With regard to the segments of *Istanbul East and West*, separated by a very small overstep (less than 1 Km), we considered two alternative scenarios, which included a single rupture of each of the segments, or a cumulative break in the course of a single event.

Through rose diagrams and histograms, compiled on the basis of the mapping of the individual branches of the fault, we carried out a quantitative analysis of the deformations along each segment analyzed, defining the prevailing modes of deformation:

• The Cinarcik segment is dominated by faults orientation pointing to N290 ° which characterize a typical trans-extensional deformation pattern (Figure 2).

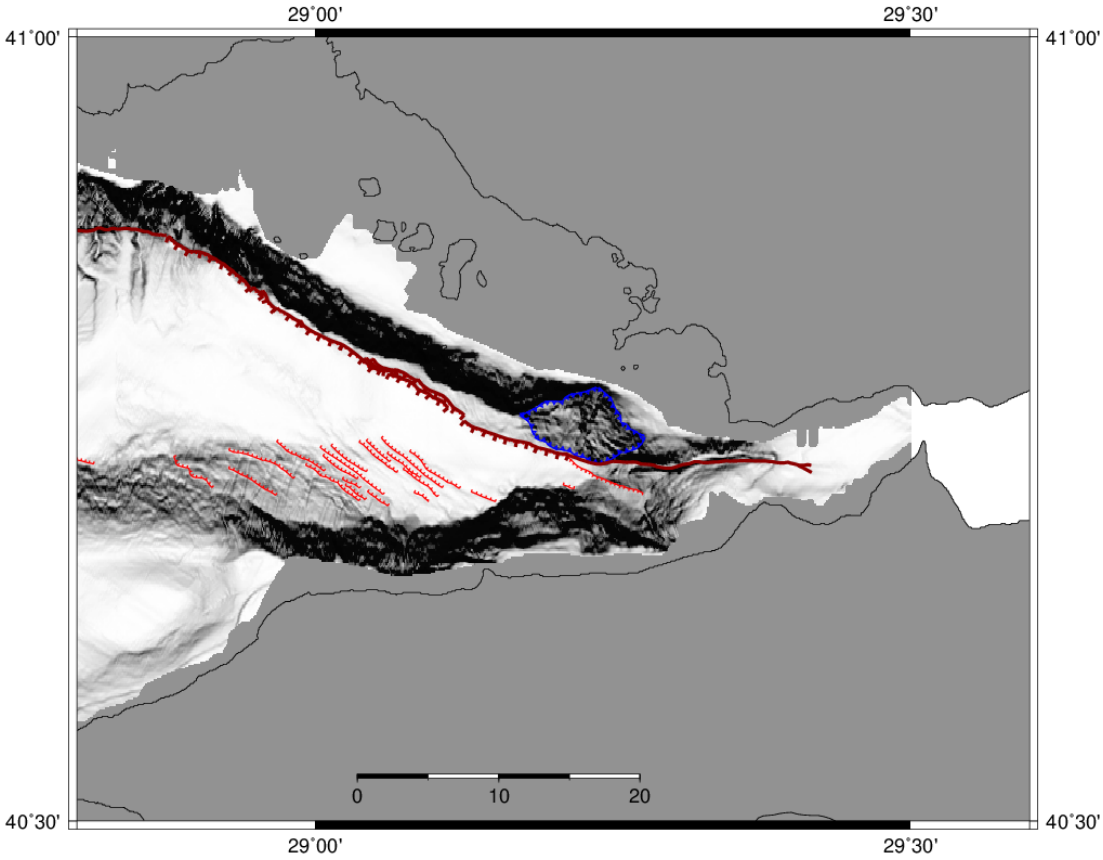

Figure 2. Morphostructural map of the Cinarcik Segment

The Istanbul East segment is characterized by the presence of strike-slip faults with orientation N270 ° and fault systems oriented N300 ° and N250 °, which represent a minor component mainly due to gravitative collapse, rather than active seismogenic.

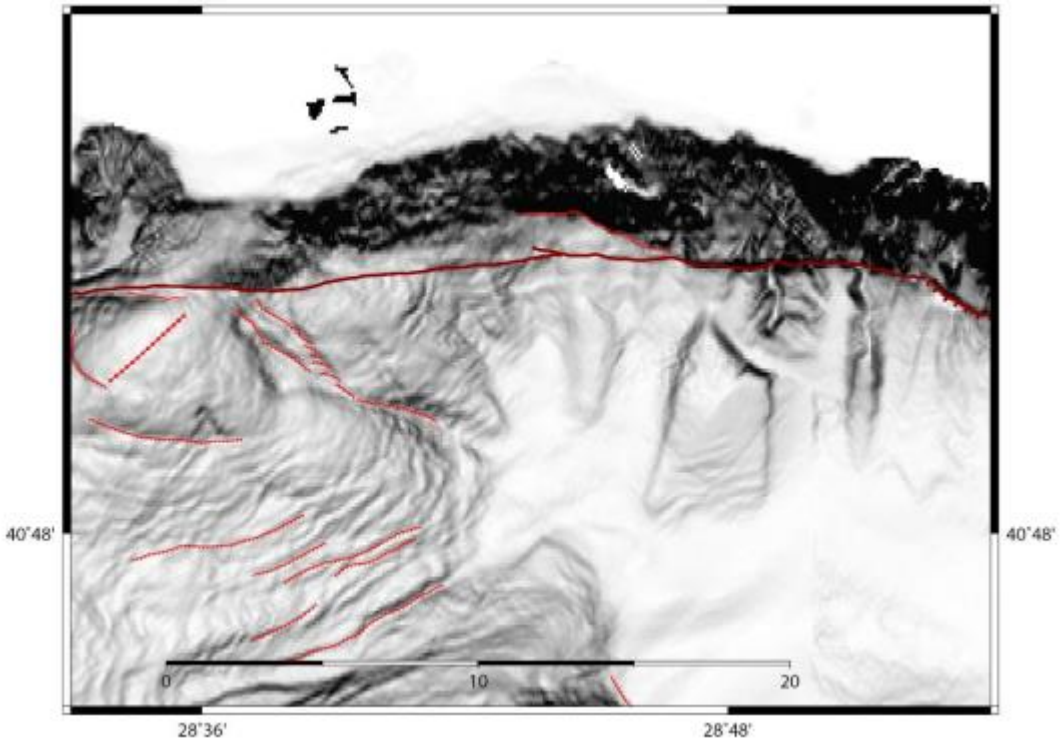

Figure 3 Morphostructural map of the Istanbul E Segment

The Istanbul West segment is characterized by two prevailing deformation modes; the longest segments are oriented N260 ° -N270 °, and accommodate mainly strike-slip deformation; the shorter segments, oriented N290 °, have trans-extensional character.

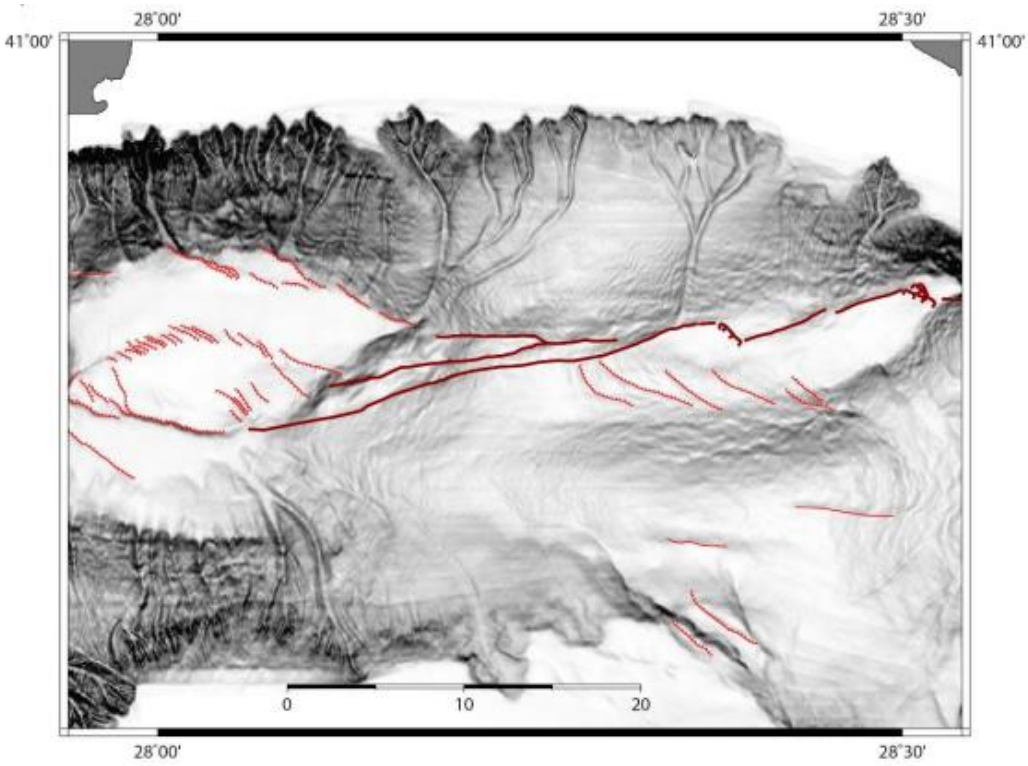

Figure 4 Morphostructural map of the Istanbul W Segment

The Tekirdag segment shows a predominantly strike-slip, with faults oriented N270 °

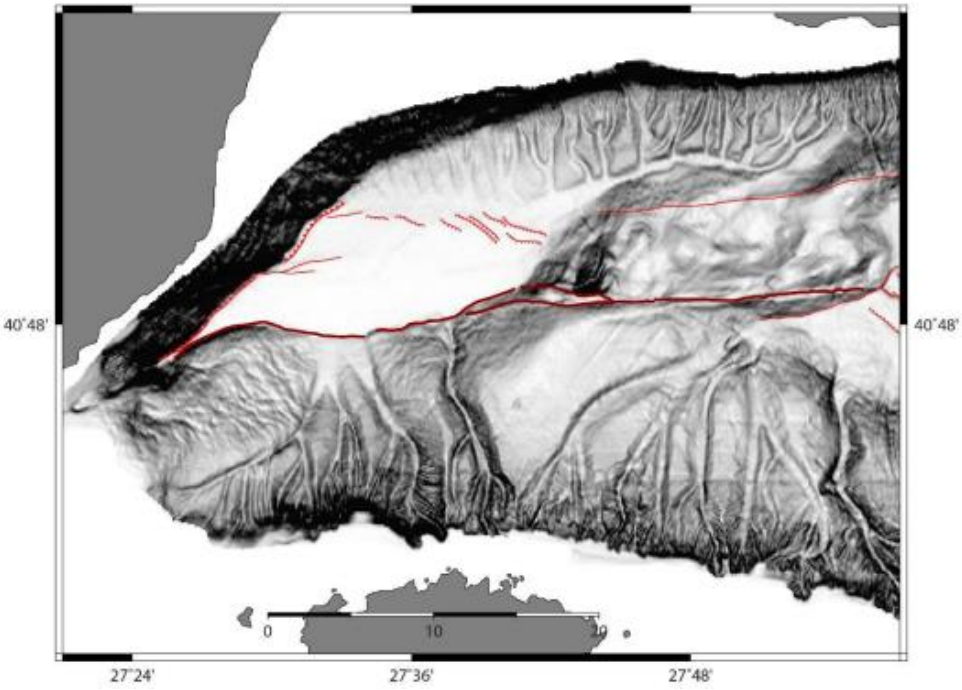

Figure 5 Morphostructural map of the Tekirdag Segment

The observations concerning the segmentation of FNA in the Marmara Sea have important implications for seismic hazard assessment in a densely populated region such as the Istanbul metropolitan area. Using the neotectonic map of Figure 1, and empirical relationships, such as that of Wells and Coppersmith (1994) it is possible to estimate the length and nature of the individual classes of active and potentially seismogenic fault (Table 1).

The expected magnitudes estimated for each segment range from 6.82 to 7.14, in the Istanbul East and the Istanbul West segments, respectively. Taking into account these two segments as a single element, we get an Mw = 7.34.As regards the other two segments, we got an Mw = 6.85 for the segment of Cinarcik and an Mw = 7.08 for the segment of Tekirdag. If we compare these results with historical catalogs (see Table 1 of Ambraseys, 1988) we find an interesting match, which confirms the validity of our structural analysis.

Table 1. Earthquakes with $M_s \geq 5.9$ in Marmara Sea area after 1899.

	Date	Origin time GMT	Epicentre N E	M_s	I_o (MSK)	r3 (km)	Location
1	1901 Dec 18	0341	39.4–26.7	5.9	VIII	220	Ayvalik
2	1903 May 26	0609	40.6–29.0	5.9	VI+	170	Marmara
3	1905 Oct 22	0335	40.6–28.3	5.9	V+	200	Marmara
4	1912 Aug 9	0129	40.8–27.2	7.4	X	500	Saros
5	1919 Nov 18	2144	39.3–27.4	6.9	IX	—	Soma
6	1924 Nov 20	2028	39.1–30.1	6.0	VII+	200	Altintaş
7	1928 May 2	2155	39.4–29.4	6.2	VIII	280	Emet
8	1935 Jan 4	1441	40.6–27.5	6.4	IX	290	Marmara
9	1939 Sep 22	0037	39.0–26.9	6.5	VIII	310	Dikili
10	1942 Nov 15	1701	39.4–28.1	6.2	VIII	230	Bigadiç
11	1943 Jun 20	1533	40.7–30.5	6.4	VIII	280	Hendek
12	1944 Jun 25	0416	39.0–29.4	6.0	VIII	225	Şaphane
13	1944 Oct 6	0235	39.6–26.5	6.8	VIII	270+	Ayvacik
14	1953 Mar 18	1906	40.0–27.5	7.2	IX	500	Yenice
15	1956 Feb 20	2032	40.0–30.1	6.1	VIII	260	Söğüt
16	1957 May 26	0633	40.6–31.0	7.0	X	460	Abant
17	1963 Sep 18	1658	40.6–29.1	6.4	VIII	320	Yalova
18	1964 Oct 6	1431	40.1–28.0	6.9	IX	400	Manyas
19	1965 Aug 23	1409	40.4–26.1	5.9	VI+	270	Saros
20	1967 Jul 22	1657	40.6–30.8	7.1	X	485	Mudurnu
21	1969 Mar 25	1322	39.1–28.4	6.1	VIII	260	Demirci
22	1970 Mar 28	2102	39.1–29.4	7.1	IX	550	Gediz
23	1975 Mar 27	0515	40.4–26.1	6.6	VII+	350	Saros

Note: M_s: surface wave magnitude; I_o+: signifies maximum observed intensity, not necessarily epicentral; r3: radius of perceptibility corresponding to I = III(MSK).
(Data from Ambraseys, 1988.)

The New Segmentation Model

This model is at the basis of a recently accepted publication on JGR, entitled "M≥7 Earthquake Rupture Forecast and Time-Dependent Probability for the Sea of Marmara Region, Turkey", by Murru et al. This model is based on the most detailed fault traces of the NAFZ branches available in the literature (Figure 6) and on their geometrical and structural arrangement at the surface. We developed a primarily characteristic earthquake rate model. An alternative model that allows multi-segment ruptures (e.g., *Field et al.*, 2014) is considered too.

This latter possibility is introduced because supported by the occurrence of historically documented *M*~8 earthquakes along the NAFZ, east of the Marmara region (e.g., 1046 *M*~7.8, 1668 *M*~7.9 and 1939 *M*~7.9).

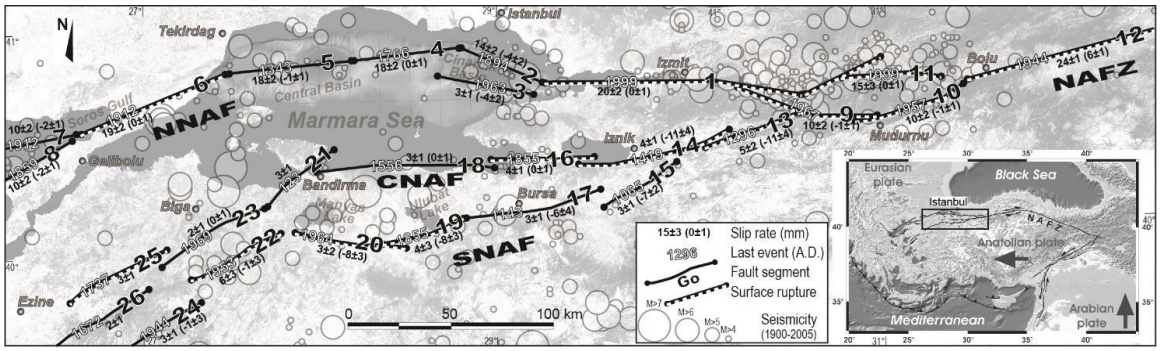

Figure 6. Synthesis of the fault segmentation model for the Marmara region. The seismic activity with M>4.0 from 01/01/1900 to 31/12/2006 for the Marmara region is shown in the background. The bold, black numbers are referred to the fault names in Table 1. The most recent event along with the strike slip rates and dip slip rates (in parenthesis) are also shown for each segment. Panel on the right show the location of the area.

We segmented the faults (Figure 6 and Table 2) on the basis of the available and reinterpreted geological and structural information at lengths near the minimum magnitude M_w~7.0. As already said, in this model also multi-segment ruptures, up to

M_w~8.0, are allowed as occurred during the 1766 events when the Central Marmara (#4) and West Marmara (#5) segments ruptured simultaneously. The maximum seismogenic depth is assumed to be 10-15 km, all segments are assumed to be near-vertical with prevalently right-lateral slip as suggested by geological, seismological and GPS data. We integrate geometrical and behavioral characteristics by introducing earthquake magnitude and slip-rates for each fault within the segmentation model and associate historical and instrumental earthquakes with the individual segments shown in Figure 6 and in Table 2. In addition, the maximum expected earthquake magnitude and the horizontal and vertical component of the slip rates are assigned for each fault segment. The rake values for each source were determined from the horizontal and vertical components of the slip rates and dip angles. The maximum expected magnitude is assigned on the basis of the implied rupture area for both single and multi-segment ruptures. The magnitude is calculated by testing different empirically derived magnitude-area relationships. Measured slip rates are very rare and with large uncertainties, in most of the cases slip rates are obtained by modelling deformation data.

More details can be retrieved in Murru et al JGR, 2016.

Table 2. Fault parameters used to build the segmentation model, for fault location refer to figure 6.

#	Fault name	Kin	Magnitude Source 50th percent.	Strike-Slip Rate (mm/yr.)	Dip-Slip Rate (mm/yr.)	L (km)	H (km)	W (km) (1σ)	strike (°)	dip (°)	Rake (°)	Last Event (AD)	Last Event (Ms)	Penultimate Event (AD)	Penultimate Event (Ms)	T-elapsed (yrs)
1	Izmit-S3	SS	7,6	20±2 *(1; 2)*	0±1 *(3)*	158 *(4; 5; 6)*	15±2,0	15,0±1,0	268	84	180	17/08/1999 *(7)*	7,4 (Mw)	25/05/1719 *(8; 9)*	7,4	16
2	Cinarcik	SS	7,0	14±2 *(2; 10)*	-4±2 *(2; 10)*	44 *(11; 12; 13; 14; 15)*	15±2,0	15,0±0,9	116	88	196	10/07/1894 *(16)*	7,3	25/10/989 *(16)*	7,2	121
3	South Cinarcik	N	7,2	3±1 *(10)*	-4±2 *(10)*	48 *(12; 13; 14; 17)*	15±2,0	16,6±1,1	283	65	233	18/09/1963 *(18)*	6,4	02/09/1754 *(9;16)*	6,8-7,0	52
4	Central Marmara	SS	7,1	18±2 *(1; 10)*	0±1 *(3; 10)*	49 *(12; 13; 14)*	15±2,0	15,1±0,9	83	84	180	22/05/1766 *(16)*	7,1	10/09/1509 *(16)*	7,2	249
5	West Marmara	SS	7,2	18±2 *(1; 10)*	-1±1 *(3; 10; 19)*	61 *(11; 12)*	15±2,0	15,4±1,0	84	78	183	18/10/1343 *(16; 20)*	7,0	23/09/1063 *(16; 20)*	7,4	672
6	Ganos	SS	7,3	19±2 *(1; 2; 10; 21; 22;)*	0±1 *(3; 10)*	74 *(21; 23)*	15±2,0	15,6±1,0	246	75	180	09/08/1912 *(9; 16; 24; 21)*	7,4	05/08/1766 *(9; 16; 24; 21)*	7,4	103
7	North Saros	SS	7,1	10±2	-2±1	46	15±2,0	15,6±1,0	76	75	191	13/09/1912	6,8	17/02/1659	7,2	103

				(1; 25)	*(3; 19)*	*(26)*						*(16)*		*(16)*		
8	South Saros	SS	7,1	10±2 *(1; 3; 25)*	-2±1 *(3; 19)*	45 *(26)*	15±2,0	15,6±1,0	241	75	191	21/08/1859 *(16)*	6,8	18/05/1625 *(16)*	7,1	156
9	Mudurnu	SS	7,2	10±2 *(1; 3; 19)*	1±1 *(19)*	70 *(27; 28; 29)*	15±2,0	15,0±0,9	291	85	174	22/07/1967 *(29, 30)*	7,2	00/00/1600 *(31)*	?	48
10	Abant	SS	7,1	10±2 *(1; 3; 19; 32)*	1±1 *(19)*	55 *(27; 28)*	15±2,0	15,0±0,0	236	85	174	26/05/1957 *(27; 33)*	7,2	17/08/1668 *(27; 33)*	7,9	58
11	Düzce -S1	SS	7,1	15±3 *(1; 34)*	0±1 *(3)*	42 *(35)*	15±2,0	15,7±1,0	262	73°	180	12/11/1999 *(7)*	7,1 (Mw)	25/05/1719 *(36)*	7,4	16
12	Gerede	SS	7,1	24±1 *(1; 3; 19; 32)*	6±1 *(3; 19)*	165 *(28; 37)*	15±2,0	15,1±1,0	261	85	166	01/02/1944 *(18; 27; 33; 38; 39)*	7,4	17/08/1668 *(27; 33)*	7,9	71
13	Geyve	N	7,1	5±2 *(1; 3)*	-11±4 *(3; 19)*	49 *(38; 40)*	15±2,0	15,3±1,0	256	78	246	01/06/1296 *(16)*	7,0	11/10/368 *(16; 27; 41)*	6,8	719
14	Iznik	N	7,1	4±1 *(1; 3; 10)*	-11±4 *(3; 19)*	74 *(38; 40; 43)*	15±2,0	15,4±1,0	259	78	250	15/03/1419 *(16; 20; 27)*	7,2	00/00/121 *(16; 41)*	7,4	596
15	Yenisehir	N	7,1	3±1 *(1; 19)*	-7±2 *(3; 19)*	40 *(38; 42)*	15±2,0	15,4±1,0	237	78	247	01/09/1065 *(16; 20)*	6,8			950
16	Gemlik	SS	7,1	4±1 *(1; 2; 25)*	0±1 *(10)*	47 *(42; 43; 44)*	15±2,0	15,4±1,0	271	78	180	11/04/1855 *(16; 20; 27)*	6,6			160
17	Bursa	N	7,1	3±1 *(1; 3)*	-6±4 *(3; 45)*	67 *(45)*	15±2,0	15,2±1,0	261	80	243	00/00/1143 *(20)*	?			872

18	South Marmara	SS	7,1	3±1 *(1; 10;47)*	0±1 *(10)*	83 *(44; 47)*	15±2,0	15,3±1,0	268	78	180	10/05/1556 *(16)*	7,2	26/10/740 *(16)*	7,1	459
19	Kemalpasa	N	7,1	4±3 *(1; 3; 19; 45)*	-8±3 *(3; 19)*	41 *(45)*	15±2,0	15,3±0,9	254	78	243	28/02/1855 *(27; 38)*	7,1	-		160
20	Manyas	N	7,1	3±2 *(1; 3; 19; 45)*	-8±3 *(19; 3; 45)*	55 *(45)*	15±2,0	15,3±0,9	282	78	249	10/06/1964 *(16; 18; 27)*	6,9	00/11/368 *(16)*	6,8	51
21	Bandirma	SS	7,2	3±1 *(3)*		41 *(28; 38; 42)*	15±2,0	16,1±1,0	231	70	180	10/11/123 *(16)*	7,0	-		1892
22	Gonen	SS	7,2	6 ±3 *(1; 3; 19; 45; 46)*	-1±3 *(3; 45)*	50 *(46)*	15±2,0	16,0±1,0	243	70	189	18/03/1953 *(16; 18; 27; 20; 38)*	7,1	00/00/1440 *(46)*	?	62
23	Biga	SS	7,2	2±1 *(1; 3; 10)*	0±1 *(10)*	57 *(28; 38; 42)*	15±2,0	16,1±1,0	241	70	180	03/03/1969 *(18)*	6,0	7/04/460 *(16; 27; 41)*	6,9	46
24	Pazarkoy	SS	7,2	3±1 *(1; 19)*	-1±3 *(3)*	54 *(28; 38; 42)*	15±2,0	16,0±1,1	60	70	198	06/10/1944 *(16)*	6,8	00/00/160 *(16)*	7,1	71
25	Can	SS	7,2	3±1 *(1)*		53 *(28; 38; 42)*	15±2,0	16,0±1,0	241	70	180	06/03/1737 (16)	7,0	00/00/155 *(16; 27)*	6,5	278
26	Ezine	SS	7,2	2 ±1 *(1; 3)*		56 *(28; 38; 42)*	15±2,0	16,0±0,9	238	70	180	14/02/1672 *(16)*	7,0			343

Reappraisal and collection of new data for the improvement of slip rates estimates and the earthquake history of the Iznik (#14) and Gemlik (#16) and Geyve (#13) fault segments.

Although the Marmara area is one of the seismic areas with the best fault data, slip rates and earthquake history of individual fault segments remain poorly constrained. On the other hand, these data are critical to produce reliable seismic hazard assessments. To improve the knowledge on these parameters is necessary to gather new geologic data. We selected the area between Geyve and Gemlik (Figure 6) to attempt to decrease the uncertainty of the slip rates evaluation and extend the record of surface rupturing earthquakes back in time. If has to be noted also that these fault segments appear to be those with the highest probability in the next 30 years.

The investigation is based on a new mapping of the main active fault segments (location in Figure 1) between Geyve and Gemlik based on the analysis of satellite imagery followed by field truthing (Figure 7). Unfortunately, we were not given permission to use aerial photographs that could have helped substantially in the interpretation at the site scale.

The fault trace is very complex and includes many strands related to the long activity history of this fault system. We focused on the most recent strand. The segmentation adopted in Figure 6 on the basis of pre-existing fault mapping does not fit completely with this new mapping, probably because we miss information from the lake bottom. The mapping allowed us to select a dozen of sites with potential for developing slip rates studies and paleoseismological trenching. Among those only three were investigated in detail (Figure 8), these are all located in the western part of the area that is more accessible. The fault trace in the eastern part of the area cut across highly vegetated and rough slopes. The fault-related topography is here very prominent and related to long-

lasting persistent tectonic activity. This diminish the potential to distinguish the Holocene deformation from the cumulated one.

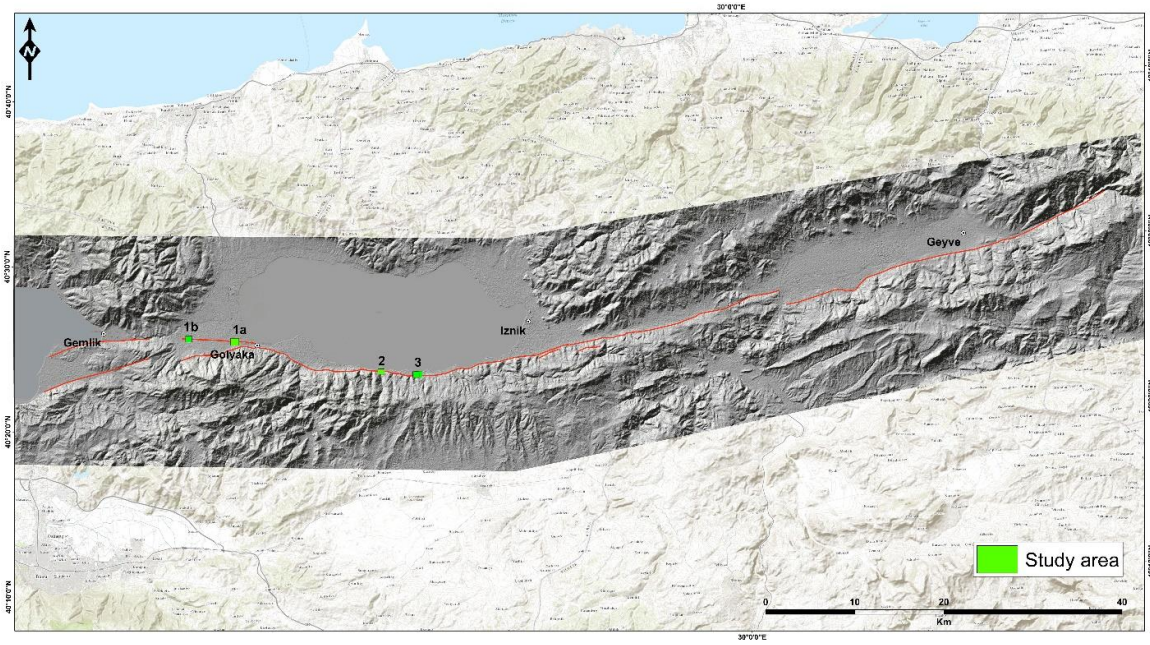

Figure 7. Mapping of the main active fault traces between Geyve and Gemlik. The green squares locate the sites that were studied in detail.

To evaluate slip rates we mapped several offset creeks by using DGPS (Figures 8,9,10). Only three of them revealed the presence of datable deposits. We sampled both for OSL and C14. Unfortunately, results are still on their way so not conclusive slip rates can be estimated but only preliminary. The maximum measured horizontal offset at the 3 sites is very comparable and varies between 60 and 75 m; thus, suggesting the main surface where the creeks developed is of the same age. Before we get dating back from the labs we can only assume that this surface postdates the LGM (<18ka); this would provide a minimum horizontal slip rate of 3 to 4 mm/yr. Interestingly, at site #3 we can compare horizontal and vertical offset as recorded by the same surface. There, the horizontal offset is 60±10m (Figure 10a) whereas, the vertical is 10±2 m (measured along the profile A-A' of figure 10). This yields a lateral and vertical slip rate of 3.4±0,5 mm/yr

and 0.5±0,1 mm/yr, respectively. The vertical slip-rate is much small than preexisting evaluations.

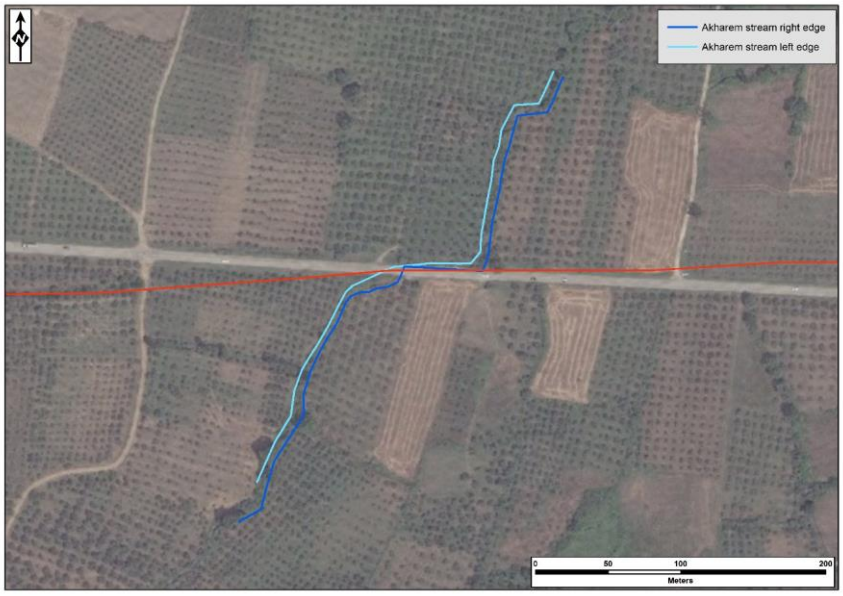

Figure 8. DGPS Mapping of creek at site #1a Akharem. A horizontal offset of 65 to 75 m can be measured at the road inflection; a minor inflection can be seen to the north. Vertical offset is 1,5 m maximum so, substantially smaller than the horizontal.

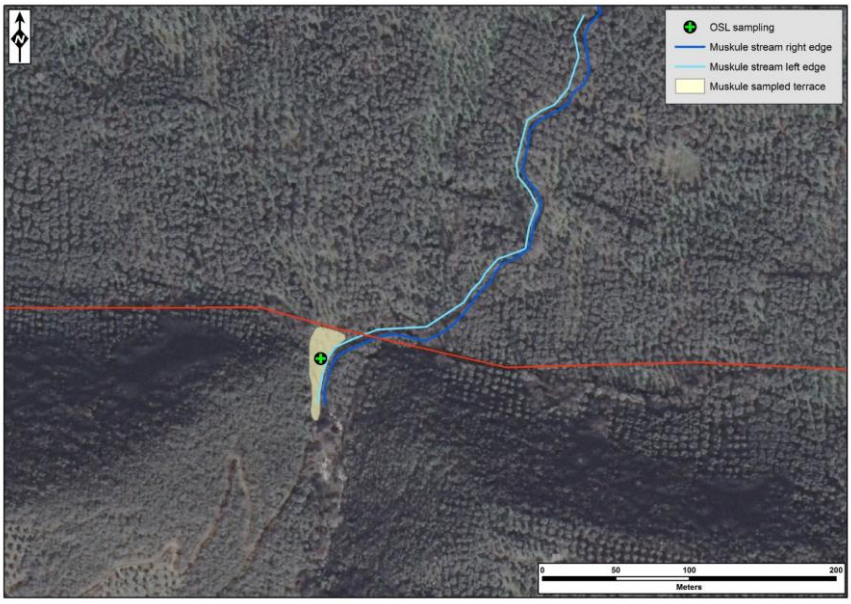

Figure 9. DGPS mapping of creek at site #2 Muskule. A horizontal offset of 60±5 m can be measured. The filled pattern on the left bank show the remnant of an alluvial surface abandoned since the creek incised the present cut. The cross symbol indicates an OSL sampling site.

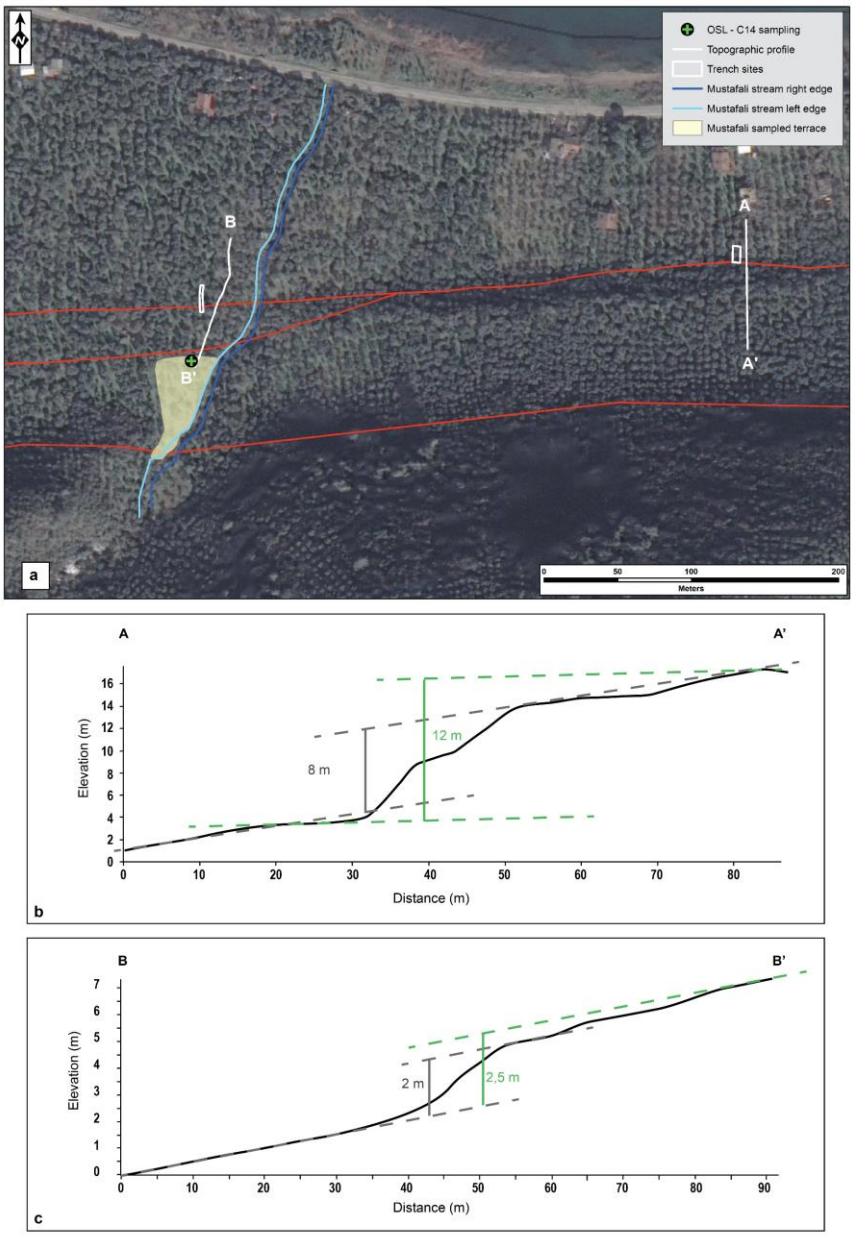

Figure 10. DGPS mapping of creek at site #3 Mustafali. A total horizontal offset of 60±10 m can be measured on a flat continuous surface that is incised by the present creek. The deformation zone is represented by two main fault strands_ the southern and older one occurs at the base of the mountain front; the northern and younger strand contains some complexity were it crosses the creek by splitting into two traces. Horizontal offset at the northern strand is of 18±2 m, whereas the vertical is about 2 m (profile B-B'). A smaller horizontal offset is recognizable further north but no fault scarp is visible there. The vertical offset increases to the east where the scarp recorded more events of deformation and reaches up to 10±1 m (profile A-A') - The filled pattern on the left bank show the remnant of an alluvial surface abandoned since this portion of the creek incised the present cut. The cross symbol indicates a OSL and C14 sampling site.

Paleoseismological Trenching

We have also excavated paleoseismological trenches at site #1b and at site #3. The intense agricultural modification has made particular difficult to choose trench sites. In most of the cases, the upper part of the section is mixed because of intense plowing since historical times.

At site #1b the trench is open on a flat alluvial surface that is interrupted by a ca. 8 km-long, EW-trending linear scarp (figure 7) that characterize the area between the Iznik lake to the east (near Golyaka) and Orhangazi Sanayi Sitesi to the west. The average height of the scarp is 2 m and many small creeks are offset across it, some of them for several tens of meters (Figure 8).

Intense farming and many factories existing in the area, the human related activities, including the maintenance and enlargement of the main road trace have modified the scarp and destroyed the fault outcrops.

The trench was 25 m–long and 2,5 m-dip, it did cross a broad scarp in an open field (figure 11) but did not intercept the fault. This is likely due to human activities that have modified the scarp, possibly retreating it to the south. However, the trench stratigraphy is very prominent (figure 12) and can be used as an input for the dating and interpretation of the offset of the Akharem stream (Site #1a - Figure 8). One OSL sample is expected to be dated in the next months.

Figure 11. View of the trench site #1b. Arrows indicate the scarp base.

Figure 12. View of the trench wall at site #1b. The stratigraphy is composed by alluvial silts, gravels and clayey-silt deposits.

At site #3, near Mustafali we excavated two trenches, one on the left bank and the other on the right bank.

The left bank trench. This trench was located in the left bank of the stream on an alluvial fan surface across one of the secondary branch of the fault. The scarp is quite broad, likely because of continuous remodeling of the surface due to agricultural activities. Across the trench, a vertical separation of the alluvial surface of about 2 m is measured. The trench strikes from N-S to NNE-SSW (to adjust to the presence of olive trees) and was 14 m-long and 2 m-dip, and exposed a sequence of alluvial fan deposits composed of gravel, sand and silt with scarce organic components suggesting a young age for all the sequence (Figure 13).

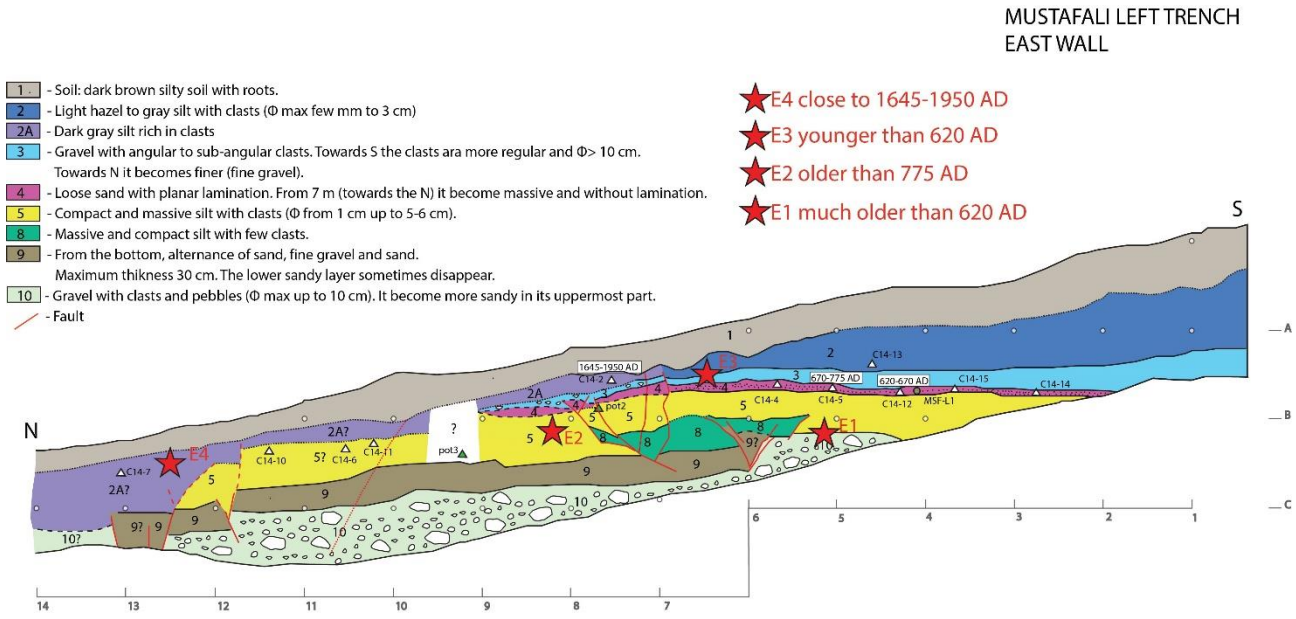

Figure 13. Log of the eastern wall of the Left bank Mustafali trench from a 1:20 field logging.

Two fault zones are exposed: one with a typical strike-slip style (between m 5 and 8) and the other with an important normal deformation (m 12-13). The analysis of the stratigraphic and structural relations suggests the evidence of 4 surface faulting events.

The relative event horizons are indicated by red stars in figure 8. Preliminary C14 dating confirms the recent age of the exposed deposits (Table 3 and Figure 13).

Table 3. *Preliminary dating from site # 3*

Sample	Material	Trench	Method	Cal.* Age (95% Prob.)
C14-5	Charred	Mustafali_SX_ew	Radiocarbon- C14	1280-1175 BP (670-775 AD)
Pot3	Pottery	Mustafali_RI_ww	Thermoluminescence	1800-1560 BP (456-216 AD)
C14-4	Charred	Mustafali_RI_ew	Radiocarbon- C14	1410-1310 BP (540-640 AD)
C14-1 + C14-3	Charred	Mustafali_RI_ww	Radiocarbon- C14	2710-2360 BP (760-410 BC)
C14-12	Charred	Mustafali_SX_ww	Radiocarbon- C14	1330-1280 BP (620-670 AD)
C14-2	Charred	Mustafali_SX_ww	Radiocarbon- C14	305-0 BP (1645-1950 AD)
MSF-1	Charred	Pit (terrace)	Radiocarbon- C14	260-0 BP (1690-1950 AD)

**present= 1950 for Radiocarbon, 2016 for Thermolunimescence*

The right bank trench. This trench is opened across a ~10 m-high scarp (Figure 10b) that displaces a much older surface including lake deposits, slope wash, colluvium. Because of the vegetation and the instability of the scarp we could excavate only its lower portion (Figures 14 and 15).

The trench exposes a very complex sequence of mixed deposits sliced by with several fault traces that produce both vertical and horizontal offset. The overall structural setting is in strong agreement with the topography of the site with a low area (graben-like) at the base of the scarp. The interpretation of stratigraphic and structural relations provides the basis to recognize evidence for at least 4 surface faulting events. The relative

event horizons are indicated by red stars in figure 14. Evidence for more events exists in the old lacustrine deposits but there is no basis to separate them in individual events (En in figure 14). C14 and TL preliminary dating provides ages that may be conflicting and needs to be integrated by more dating (Table 3 and Figure 14).

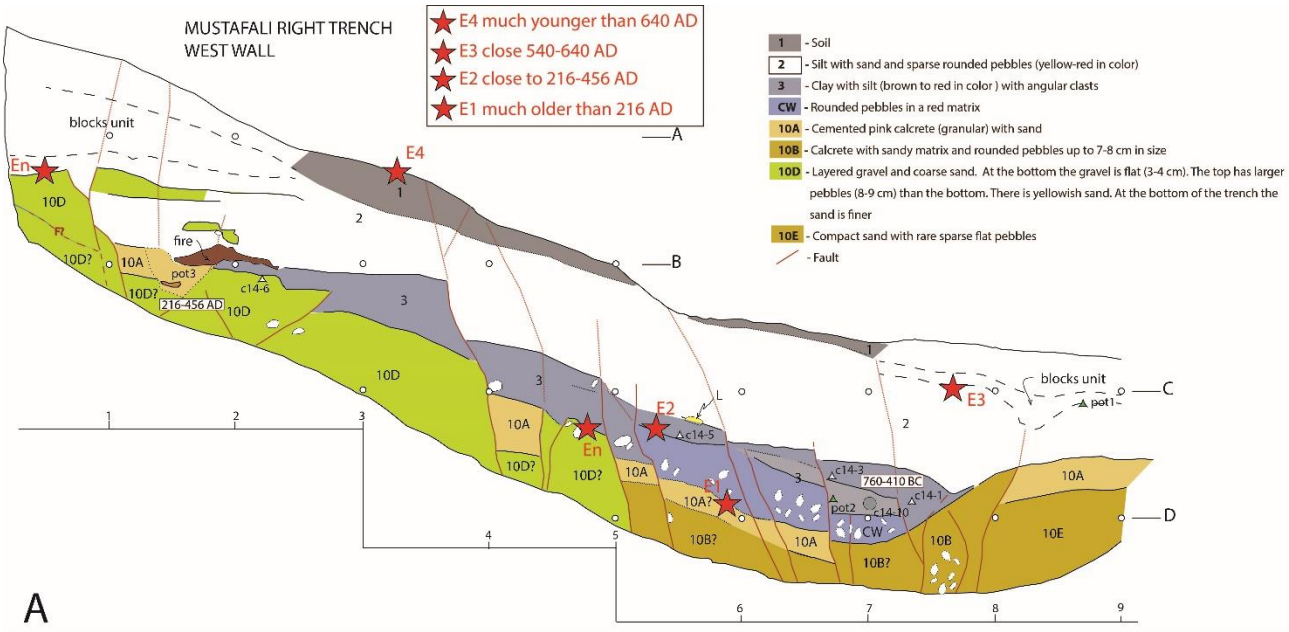

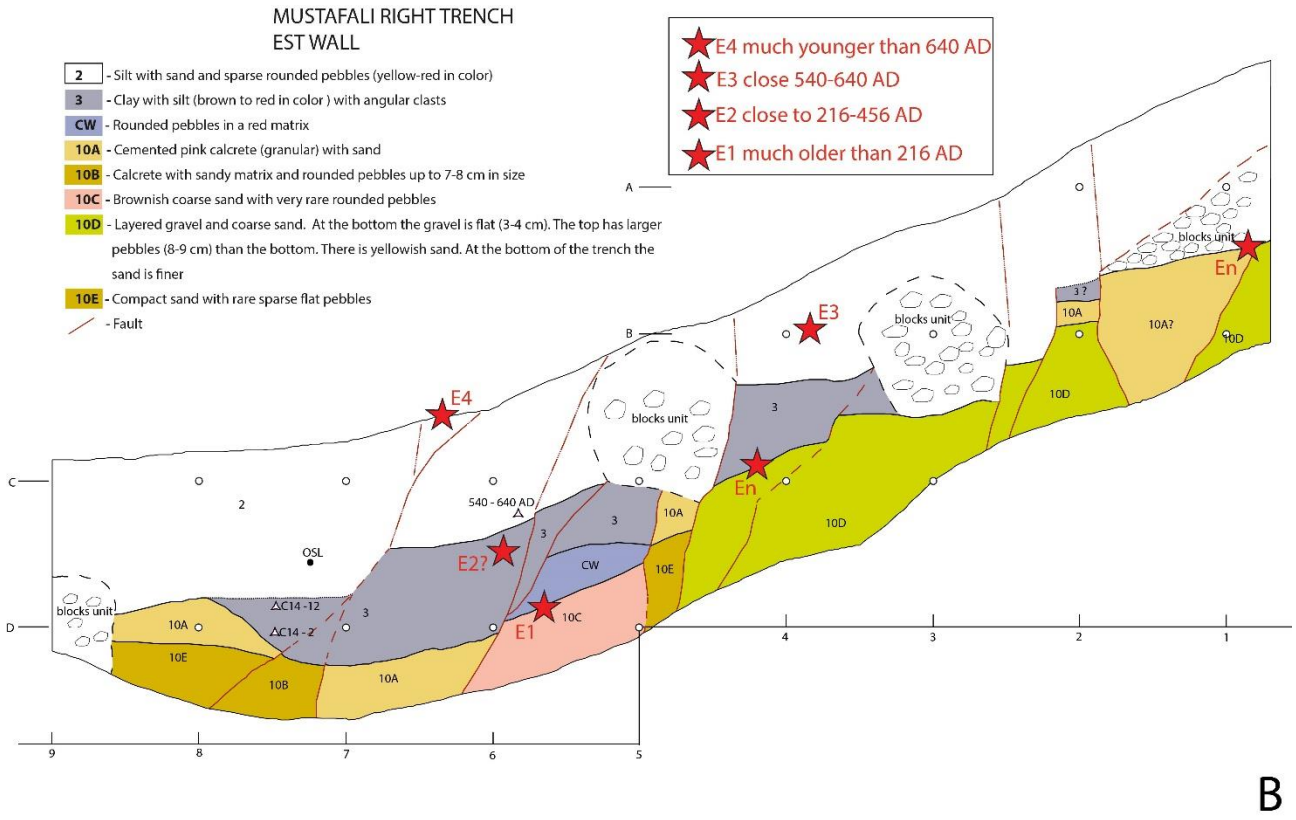

B

Figure 14. Log of the western wall (A) and eastern wall of the Right bank Mustafali trench from a 1:20 field logging.

By merging results from both trenches at site # 3 we provide preliminary dating of the 4 most recent surface faulting events. These should be considered a minimum as faulting might have occurred also along different branches of the fault at the surface.

From published literature the most recent events along the Iznik and Gemlik fault are the 1419 AD and 1855 earthquakes, respectively. From our results this is not confirmed but it is possible. Because of the location of the site, near the overlap zone of the two faults that is very narrow, we should also consider that both events produced surface faulting at this site and thus that the 1855 overprinted the 1419.

Event	Trench RIGHT	Trench LEFT	Converging Age (this work)
Event 1	much older than 216 AD	much older than 620 AD	Pre 216 AD
Event 2	close to 216-456 AD	older than 775 AD	Close to 216-456 AD
Event 3	close 540-640 AD	younger than 620 AD	620-640 AD
Event 4	much younger than 640 AD	close to 1645-1950 AD	Close to 1645-1950 AD

Figure 15. View of the Right bank Mustafali trench (site #3) from north.

Offshore Paleoseismology

The use of subaqueous sedimentary sequences in marine and lake basins as archives of past earthquake events is part of a newly evolving field of subaqueous paleoseismology (e.g., Beck et al., 1996, 2007; Chapron et al., 1999; Arnaud et al., 2002; Goldfinger et al., 2003; Schnellmann et al., 2005; McHugh et al., 2006; Sarı and Çağatay, 2006; Carrillo et al., 2008). Such studies are important for seismic risk evaluation, providing important information on fault segmentation and recurrence time. An important area of study in subaqueous paleoseismology is the establishment of criteria for distinguishing turbidites of seismic origin from those of other origins, such as storm waves, hyperpycnal flows, gas hydrate dissociation, sediment overloading, volcanic eruptions and floods (Postma et al., 1988; Prior et al., 1989; Nemec, 1990; Mulder and Syvitski, 1995; Beck et al., 1996, 2007; Chapron et al., 1999; Cita and Aloisi, 2000; Nakajima and Kanai, 2000; Shiki et al., 2000; Arnaud et al., 2002; Goldfinger et al., 2003; Schnellmann et al., 2005; Carrillo et al., 2008). Long-term paleoearthquake history of faults is important for probabilistic earthquake risk assessment. Such records can be obtained from the study of mass-transport units triggered by seismic activity in marine and lake basins.

The Sea of Marmara (SoM), located on the North Anatolian Fault (NAF), is an important laboratory for the study of paleoearthquake records, mainly because it has: a) more than 2500 years of historical earthquake records with which radiometrically dated sedimentary earthquake records can be correlated, b) high sedimentation rates (≤ 3m /kyrs) so that individual events can be distinguished, and c) cold fluid and hydrocarbon seeps along active faults, leaving sedimentary and geochemical signatures of earthquake activity. After the destructive 1912 Mw 7.4 Mürefte and 1999 Mw 7.4 Izmit and Mw 7.2 Duzce earthquakes, the SoM represent a seismic gap. It is therefore crucial to obtain

information on the long-term earthquake history of the NAF in the SoM. In the deep part of the Sea of Marmara (Turkey), the sedimentation developing upon the NAF is strongly influenced by the associated seismic activity, through gravity reworking (fluidized landslides) and tsunamis. Specific layers (homogenites+turbidites, HmTu), representing individual sedimentary events, have been characterized along various piston cores retrieved from the different subbasins of the SoM (Beck et al., 2007, McHugh et al., 2006, 2014; Eriş et al., 2012; Drab et al., 2012, 2015; Çağatay et al., 2012; Campos et al., 2013). In the Sea of Marmara, there have been many attempts for the last few years to carry out a systematic studies on piston cores recovered from the various Marmara basins. These researches aim to characterize the different segments of the NAF, using high resolution digital X-Ray Radiography and μ-XRF Core Scanner, MSCL physical properties, grain-size analyses and also anizotrophy of magnetic succeptibility.

Definition of seismoturbidites in the Sea of Marmara

Strong ground shaking from rupture of earthquakes has been inferred to trigger turbidity currents that potentially leave a very long record of past earthquakes in the form of turbidites (Shiki et al., 2000; St-Onge et al., 2004; Goldfinger et al., 2012). Turbidite paleoseismology uses combined evidences from sedimentology, tests of synchroneity, stratigraphic correlation, and analysis of non-earthquake triggers to develop a reliable earthquake record for submarine fault zones (Goldfinger et al., 2012). Within the past ten years, much progress has been made in the field of submarine paleoseismology, understanding processes linking submarine earthquakes with sedimentation events and developing techniques for addressing earthquake recurrence intervals and segmentation of fault systems. Exploration of submarine mass-wasting events and related turbidite paleoseismology in the SoM has been a newly evolving field of subaqueous

paleoseismology due to seismic risk evaluation that provided important informations on fault segmentation and recurrence time of earthquakes along the NAFZ.

Definition of seismoturbidites on studied cores from the Sea of Marmara is mainly based on visual core descriptions that involve lithologic observations such as colour, bedding, sedimentary structures and disturbances, grain size distribution, texture, bioturbation and fossil content. In many researches regarding to investigate seismoturbidites in the SoM, various sedimentological tools and approaches have been published (Çağatay et al., 2012; Drab et al., 2012; Eriş et al., 2012; Campos et al., 2013; McHugh et al., 2014; Beck et al., 2015), only results (data and interpretations) implying paleoseismological aspects will be envisaged. The descriptions of seismoturbidites on cores have been refined by using X-ray radiograms, granulometric data, magnetic susceptibility measurements and XRF-scanning data. To constrain the depositional pattern of the major turbidites, their textural characteristics are accessed by computing distribution parameters like mean, sorting, skewness. But several other types of mass movement deposits (MMD) are potentially related to paleoearthquakes: slumps, debrites, graded turbidites, matrix supported turbidites and homogenite type turbidites (Grall et al., 2014). In order to construct consistent age models for seismic risk evaluation and recurrence time, the distinction between instantaneous deposits (background sediments) and hemipelagic deposits is crucial. A new method of Anisotropy of Magnetic Susceptibility has been recently used in order to differentiate seismoturbidites from climatic-induced turbidites in cores (Campos et al., 2013; Beck et al., 2015). This method was successfully applied to the core sediments obtained from the Çınarcık Basin. In homogenites, a particular settling of magnetic and argillaceous particles is observed

through a very high magnetic foliation inconsistent with compaction by overlying sediments.

The successions of piston cores recovered from the subbasins of the SoM display numerous turbidites, often associated with an overlying homogenite, which are intercalated with background sedimentation (Beck et al., 2007, 2015; Eriş et al., 2012; Fig. 16). It is represented in the whole core by a hemipelagic silty clayey mud. Although the word “hemipelagite” should be restricted to marine/oceanic deposits, we also use it for the nonmarine succession as, in both cases, it is a mixture of clayey silty terrigenous fraction (clay minerals, quartz, plagioclase, amphibole, pyroxene, fresh micas, opaques) and planktonic biogenic or bioinduced particles (carbonate and silica: calcareous nanoplankton, diatoms). They have been observed in the three basins (Tekirdağ, Central, Çınarcık) with identical characteristics and occurrence frequency (Beck et al., 2015). These layers can be related to in situ slight reworking by the episodic increase of bottom current velocities. A minor part of these intervals show low-angle microprogradation (flaser-bedding type) and appear associated with homogenites; thus, they are included into instantaneous gravity reworking events.

Regarding to published studies on turbidite-homogenite deposits (TH) triggered by earthquakes in the SoM, they have the following characteristics: (1) the basal layer of the turbidites often shows multiple pulses, and (2) grain size change between the sand and the silt sublayers is abrupt, (3) change in grain size, sorting and skewness can also be abrupt in the silt and clayey silt sublayers, whereas the decrease in kurtosis is generally gradual. The top clay rich part of the turbidite is marked by a minima in sorting and a skewness around zero. The basal TH parts have high gamma density and magnetic susceptibility, and are often enriched in one or more of elements, such as Si, Zr, Ca, Ti, K

and Fe, indicative of coarse detrital and carbonate shell input (Figs. 17 and 18). Manganese (Mn) shows a sharp increase just below the basal sandy sublayer. The transition to the hemipelagic sedimentation is marked by a rising until a maximum in K, Ca or in Ca/Ti ratio. These elements do occur in proportion to the hemipelagic sedimentation. Minor turbidites do not have a noteworthy XRF signature.

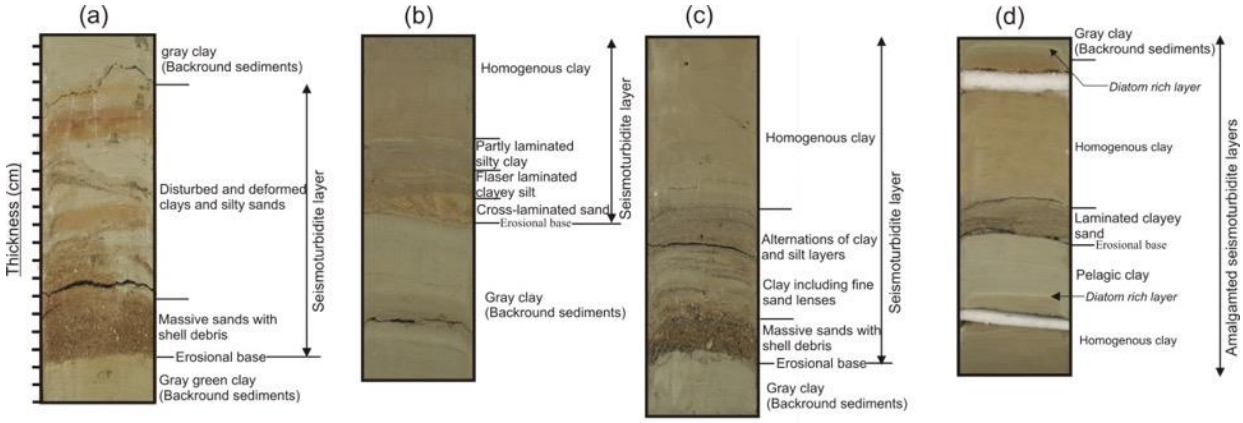

Figure 16. Lithological and textural properties of seismoturbidites defined from the Çınarcık Basin (Eriş et al., 2012).

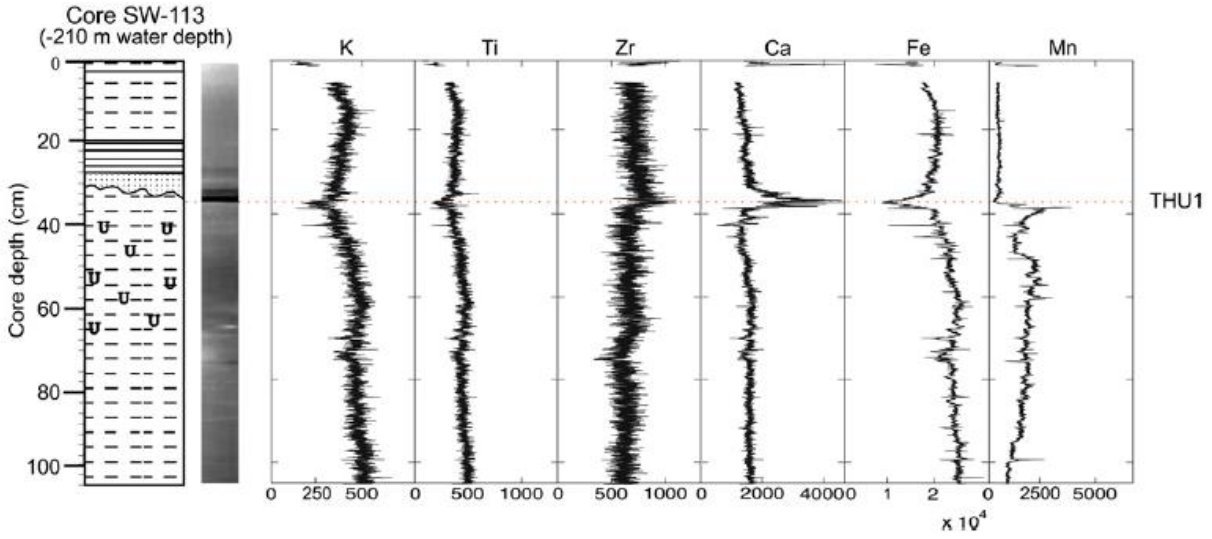

Figure 17. Geochemical elemental composition through the seismoturbidites in short core recovered from İzmit Gulf that is studied by Çağatay et al. (2012).

For historical and older events, the seismic origin of a specific layer can be established as follows:

- directly, using intrinsic characteristics such as texture, origin of components, overall geometry, etc. (Beck et al., 2015);
- indirectly, (i) on the basis of correlations with reported seismic events (for historical seismicity) (e.g., Siegenthaler et al., 1987; Piper et al., 1992; Chapron et al., 1999; Goldfinger et al., 2007; Beck et al., 2012) and
- when detecting the same paleoevent in a large area independently from local setting (e.g., variable slope dip). This second approach is especially used for deep structures, as subduction, (e.g., Goldfinger et al., 2007; Gracia et al., 2010; Moernaut, 2011; Pouderoux et al., 2012) and also, in some cases, for surface-reaching major faults (e.g., Goldfinger et al., 2007);
- combining both types of arguments.

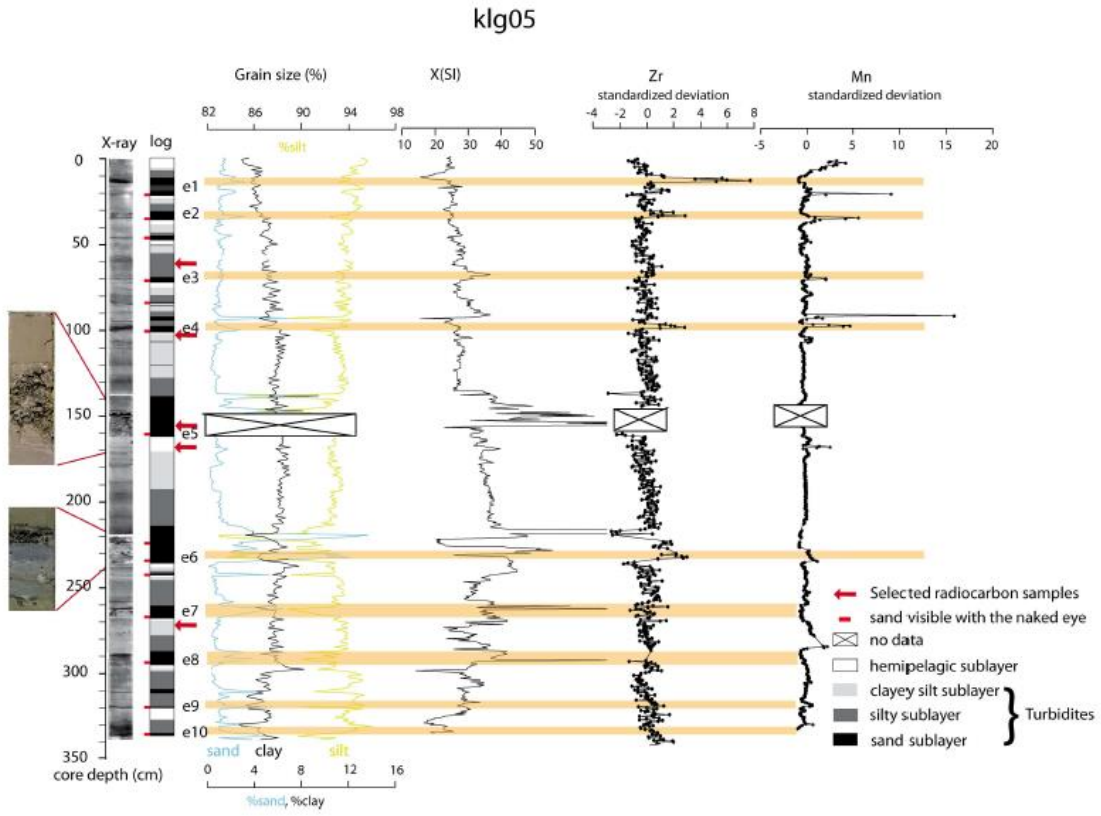

Figure 18. Stratigraphic log of the Klg05 core in the Tekirdağ Basin obtained by combining X-ray imagery, grain size, magnetic susceptibility data, Mn and Zr standardized intensities (Drab et al., 2012). Main deposited turbidites are identified and labelled; event labels change according to their stratigraphic position, beginning with 1 at the top of the core.

The seismic studies from the SoM can provide to differentiate seismoturbidite layers with its lateral extent based on the characteristic of reflection configurations (Eriş et al., 2012). The effects of seismo-tectonic activity is evident from seismically transparent or internally chaotic mass-wasting units (Figs. 19 and 20). On the eastern part of the Tekirdağ Basin, seismic profile displays a presence of a transparent lenticular layer below the marine (Unit-1) sediments (Fig. 20). This lens bear all the typical seismic characteristic of deposit resulting from the failure of submerged marine slope. It was deposited in front of the failured scar on SW corner of the profile and its thickness reaches about 25 m.

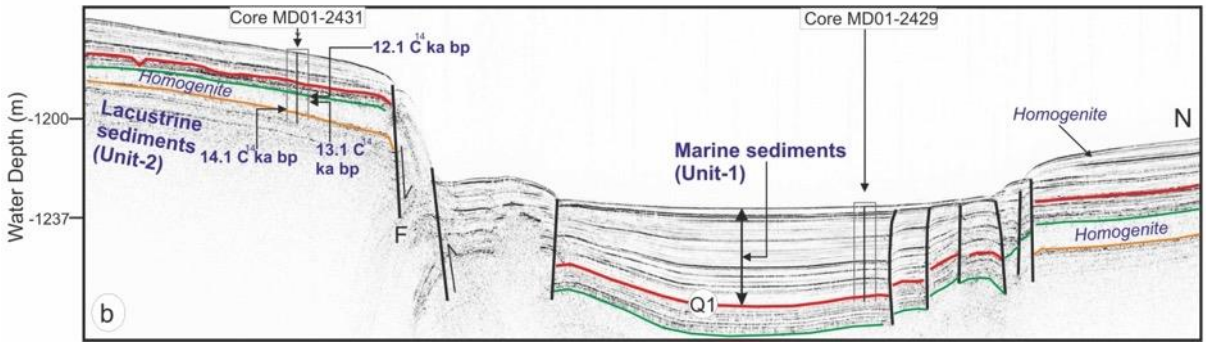

Figure 19. High-resolution (3.5 kHz Seismic profile Cb04 across the Central Basin, showing a nearly 8 m-thick 'homogenite' layer calibrated by radiocarbon dates from piston Core MD01-2431 (Eriş et al., 2012).

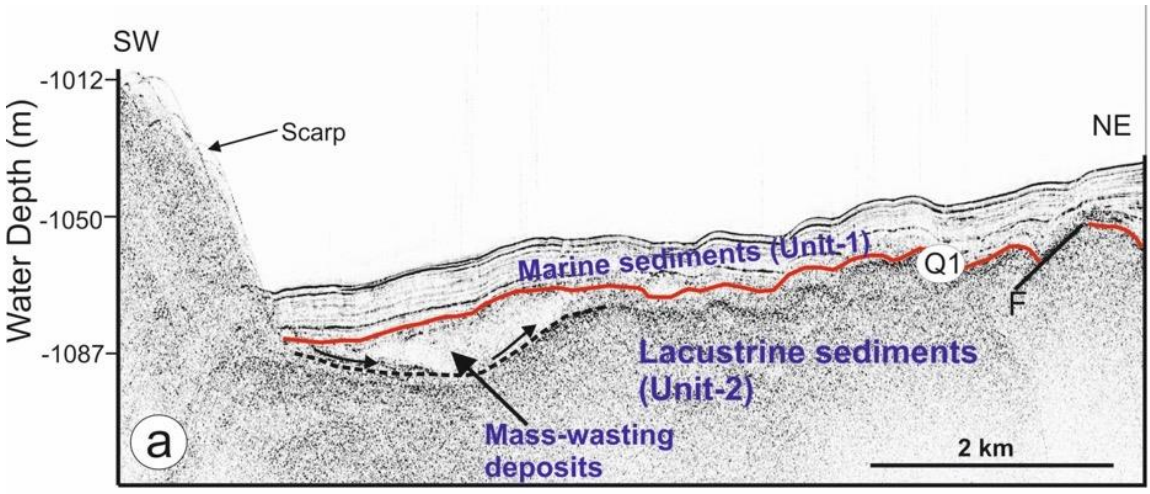

Figure 20. High-resolution (3.5 kHz) seismic profile T26 at the eastern side of the Tekirdağ Basin, showing evidence for a mass-wasting deposit below the marine sediments (Unit-2). Surface Q1 separates the marine (Unit-2) and lacustrine (Unit-1) units, and is dated to 12.3 cal ka BP (Eriş et al., 2012).

For the subaqueous records, two major groups of effects can be detected and analyzed: (i) in situ post-depositional disturbances (Grall et al., 2012; Campos et al., 2013; Beck et al., 2015; McHugh et al., 2014), and (ii) gravity-driven reworking and resettling of large masses of unconsolidated sediments (Eriş et al., 2012; Çağatay et al., 2012). Two major questions arise for both groups: (1) how to ensure the earthquake-triggering, (2) how to identify the responsible active structure(s). For in situ disturbances, the first problem is generally solved; in particular, it benefits from analogical and/or numerical modeling (e.g., Moretti et al., 1999; Wetzler et al., 2010). For redepositional processes which are envisaged in the present work–several recent catastrophic events could be surveyed shortly after their occurrence (Thunell et al., 1999; McHugh et al., 2011; Lorenzoni et al., 2012); the results reinforced the earthquake induced interpretation proposed for some "homogenite-type" layers (Beck et al., 2015). Previous studies mostly conclude that (1) significant turbiditic deposition directly related to earthquake shaking occurs in the Marmara Basin (Beck et al., 2015; Grall et al., 2012), (2) basins' filling is

mainly controlled by active faults (Beck et al., 2015; McHugh et al., 2014) and may document earthquake rupture along the associated fault segments, and (3) seismoturbidites are associated with oscillating bottom currents (seiche), with variable suspended load or bedload (Eriş et al., 2012; Beck et al., 2015).

Co-seismic data obtained from the deep-basins of the SoM

Within the framework of the 3 years of continuous collaboration between different research groups, submarine paleoseismological studies in the Sea of Marmara have produced useful results (Çağatay et al., 2012; Eriş et al., 2012; Drab et al., 2012; Beck et al., 2015; Campos et al., 2013; Grall et al., 2014; McHugh et al., 2014). The offshore paleoseismological studies in the SoM have been mainly focused on the deep subbasins and ridges with various water dephs. However, regarding to connection with the SoM, İzmit Gulf has been studied to evaluate for paleoseismologic evidences due to NAFZ activity deforming the gulf itself (Çağatay et al., 2012). The dated sediments obtained from the studied all cores span nearly the last 16 ka BP, but mostly covering the time period of Holocene. As discussed in many researches, the deteriotion on paleoenvironmental conditions have been investigated during the last few tens of thoushand years because of paleoclimatic and eustatic changes in the SoM, together with water exchanges between the Black and Mediterranean seas (Aksu et al., 1999; Çağatay et al., 2000, 2009, 2015; Eriş et al., 2007, 2010; Hiscot et al., 2002; McHugh et al., 2006; Vidal et al., 2010).

Based on these paleoenvironmental changes, the stratigraphy of the Marmara sediments has been well established that is commonly consistent with the global isotope stratigraphy regarding to glacial and interglacial periods during the Late Quaternary. In the SoM, the nonmarine–marine transition has been investigated as a chronological

marker reliable for precise correlations. Due to its importance for the studies of the last climatic cycle, the hydrologic evolution of the SoM has been intensively surveyed by different authors through sedimentation. The SoM was converted from lake to marine at 12.8 ka BP (Çağatay et al., 2015) when the prominent paleoenvironmental changes took place, regarding to its hydrology, geochemistry and paleoecology. The effects of these changes on the stratigraphy have been well-known, but their role on the deposition of seismoturbidites in the subbasins of the SoM has not been executed very well yet. Combining all published results about underwater paleoseismology in the SoM, a few saticifactory hypotheses still appear to be questionable. The differences between the nonmarine and marine with respect to seismoturbidite texture and its occupying related with the background sedimentation provide to correlation some criteria based on the thickness, geochemical properties, biogenic and bioinduced markers (Eriş et al., 2012; Campos et al., 2013, Beck et al., 2015). Moreover, episodes of widespread mass wasting have occurred in the SoM near the end of the last glaciation (Eriş et al., 2012) as well as during previous cycles (Grall et al., 2014). Understanding their relationships with sea-level variations and marine-lacustrine transitions would improve our understanding of environmental factors influencing slope instability and, thus, seismoturbidite records.

The oldest depositional sequence for distinguishing seismoturidite layers have been published from the Çınarcık and Central basins of the SoM (Eriş et al., 2012; Campos et al., 2013; Beck et al., 2015). A giant RV Marion Dufresne piston core MD01-2425 recovered from the 1276 m-deep Çınarcık Basin of the SoM documented characteristics of deep basin sedimentation influenced by large-scale gravity-controlled mass-wasting processes and associated turbidite deposition during the Late Pleistocene to Holocene (Fig. 21). In Eriş et al. (2012), they presented detailed stratigraphic and sedimentological

descriptions and textural properties of Core MD01-2425, involving laser particle-size, magnetic susceptibility and AMS ^{14}C analyses. They attempted to correlate possible major mass flow events that occurred in the Çınarcık and Central basins during the Late Pleistocene to Holocene. On the basis of lithologic analysis and together with textural characterization of Core MD01-2425 from the Çınarcık Basin, the core sediments contain twenty major seismoturbidite layers ranging from 20 cm to 200 cm in thickness, that are labeled in this study from TU-1 to TU-20 (Eriş et al., 2012; Fig. 22). The lithology and texture of these seismoturbidite layers imply that they mostly begin at the base with massive and finely-laminated sand and silt over a sharp basal erosional contact (Fig. 23).

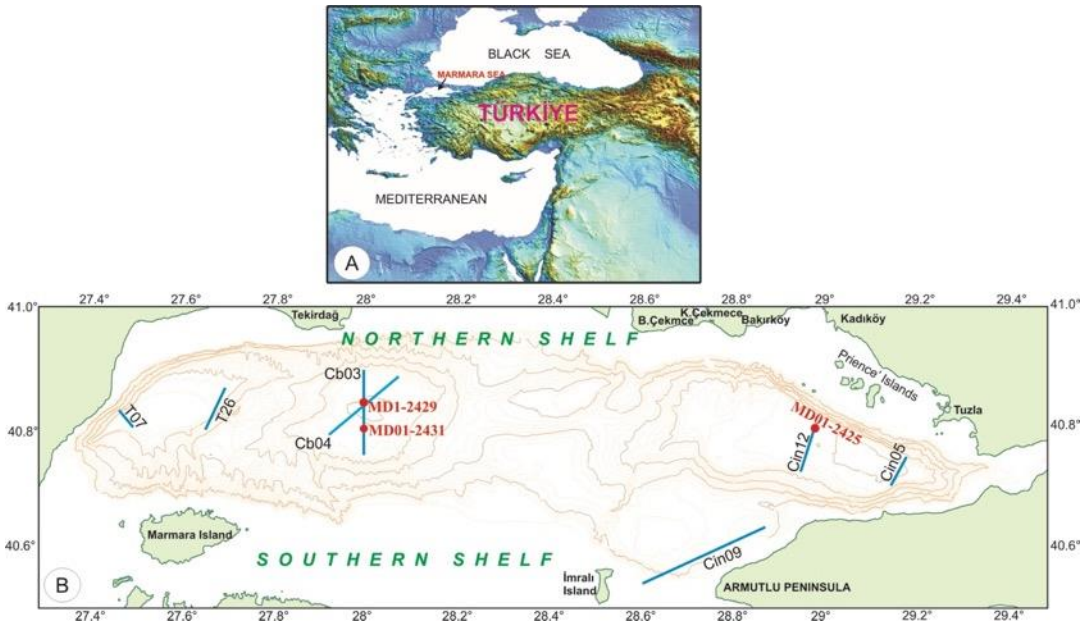

Figure 21. Location map showing cores studied by Eriş et al. (2012) and also seismic chirps on the core locations.

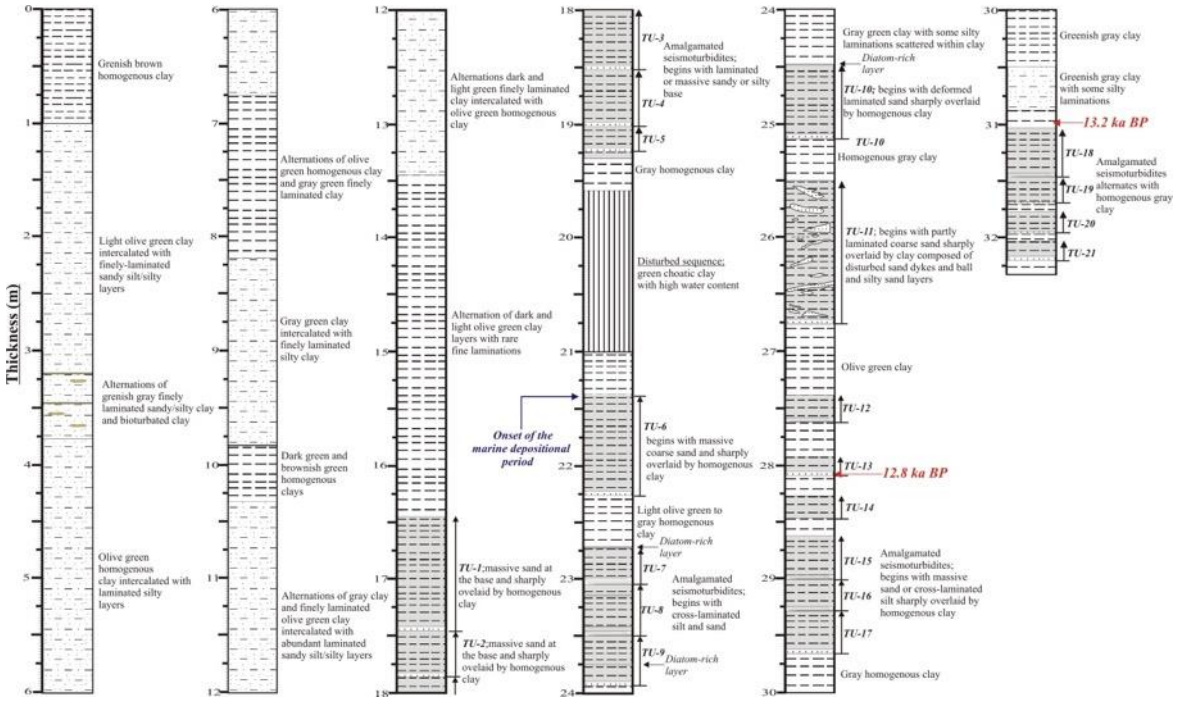

Figure 22. Summary of lithostratigraphic subdivisions of Core MD01-2425 located on the Çınarcık Basin (Eriş et al., 2012). The seismoturbidite layers (>20 cm thick) (labeled here as TU-1 to TU-20) mainly dominate in the lower part of the marine sediments (Unit-2), whereas the lacustrine sediments (Unit-1) are composed of alternating seismoturbidite layers and hemipelagites.

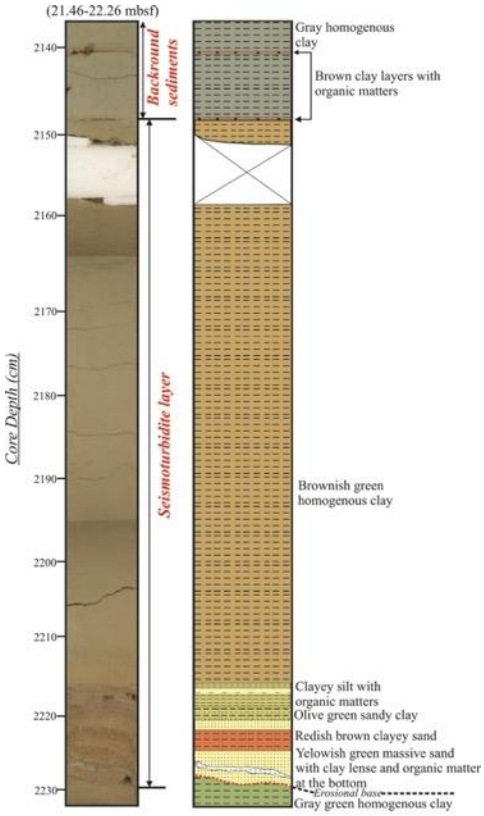

Figure 23. Detailed view and simplified log of the selected seismoturbidite layer (TU-6) between 21.46 and 22.26 mbsf in Core MD01-2425 (Eriş et al., 2012). This layer comprises two different lithological parts; the coarse-grained lower part that is sharply overlain by the homogeneous upper part. mbsf, meters below seafloor.

Eriş et al. (2012) also documented existence of 8 m of major mass-wasting event that presumably took place prior to connection to the Mediterranean water at 12.8 ka BP. The most significant imprint of a mass-wasting event has been previously investigated by Beck et al. (2007) from the Central Basin of the SoM. The sedimentary record of this synchronous seismic event from the Çınarcık Basin is also shown both by seismic and core data (Figs. 18 and 24). Core MD01-2425 from the Çınarcık Basin exhibited the volume differences (or thickness differences) of the seismoturbidite layers between the marine (Unit-2) and lacustrine (Unit-1) parts of the core. This can be related to a combination of the number of induced mass-wastings and size of slope failure in the Çınarcık Basin (Eriş et al., 2012; Campos et al., 2013). These are initially governed by climatic and water level changes during the Late Pleistocene to Holocene.

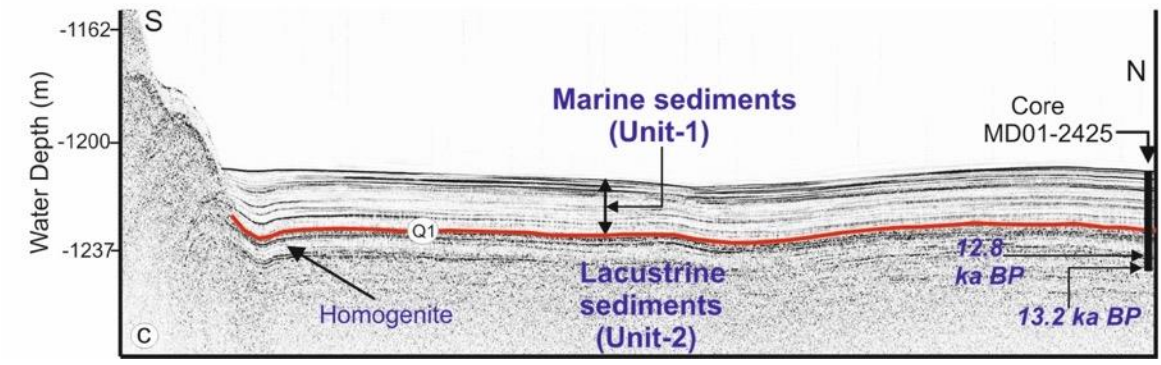

Figure 24. Seismic profile Cin12 across the Çınarcık Basin, showing a thick (2 m) 'homogenite' layer below the marine sediments (Unit-2) that are penetrated by piston Core MD01-2425 (Eriş et al., 2012).

Recently, the seismoturbidite deposits from the Çınarcık and Central basins have been extensively studied by Campos et al. (2013) and Beck et al. (2015) in order to

investigate detailed criteria for differentiating these special layers by using sedimentological properties in Core MD01-2425. Campos et al. (2013) focused on the use of AMS (Anisotropy of Magnetic Succeptibility) to characterize re-depositional processes in Çınarcık Basin directly related to active faulting and undergoing frequent strong earthquakes during the Late Pleistocene to Holocene. The magnetic foliation of homogenites in Core MD01-2425 (Fig. 21) is clearly distinct from the one displayed by hemipelagites, both for marine hemipelagites and for similar lacustrine fine-grained sediments ("hemipelagites" in a broad sense). The deduced strong planar horizontal array of homogenites fits with the hypothesis of a specific settling (Beck et al., 2007; Eriş et al., 2012): strong initial segregation from gravity-reworked soft sediments under oscillatory conditions, long lasting to almost stablere-suspension of fine fraction, "ponding" in deep basins subdivisions. As this process has been related to earthquake-triggering in isolated basins (see Introduction), the use of AMS for subaqueous paleoseismology appears reinforced. On the same core (MD01-2425) from Çınarcık Basin, Beck et al. (2015) produced age-depth model with additional ^{14}C dates to obtain more precise chronology of the core sediments (Fig. 25), and therefore, they managed to establish chronostratigraphic correlations between the Çınarcık Basin (core MD01-2425) and the Central Basin (cores MD01-2429 and MD01-2431). Based on these correlations they concluded that the general chronostratigraphy, appear very similar between the three cores (Fig. 26).

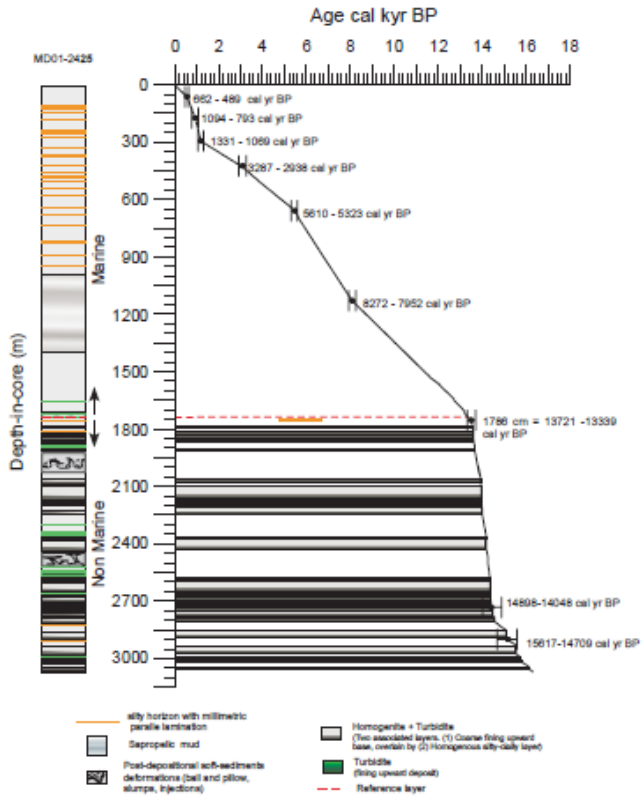

Figure 25. Age/depth curve of core MD01-2425 (Çinarcik Basin), displaying major instantaneous deposits (homogenite+turbidite).Red dashed line indicates the limit between nonmarine (below) and marine sequences;pLGH: pre-late glacial homogenite (Beck et al., 2015).

According to Beck et al. (2015), the detailed sedimentological observations on Core MD01-2425 provided to examine the contrast between the two parts of the succession (roughly between late glacial and Holocene) regarding to presence of seismoturbidites. They concluded that the abundance of terrigenous input in the late glacial may due to either higher storage of sediments in subaqueous deltas and subsequently higher potential for gravity reworking (climatic influence), or more frequent and powerful earthquakes (tectonic influence). For the SoM, a change in the water density vertical profile and in circulation may also account for the distribution of bedload and suspended load. In order to extract a paleoseismic record through turbidite-homogenite events, they checked (1) a

regional correlation between the Central and Çinarcik basins (MD01-2425, -2429, and -2431; see also Beck et al., 2007; Eriş et al., 2012), and (2) a more localized correlation on both sides of the active scarp bounding the inner Central Basin on its southwestern side. The comparision of cores (MD01-2429 and MD01-2431) from the Central Basin demonstrated that the high difference of mean sedimentation rates between the two sites was essentially due to the difference of instantaneous sedimentary event thicknesses.

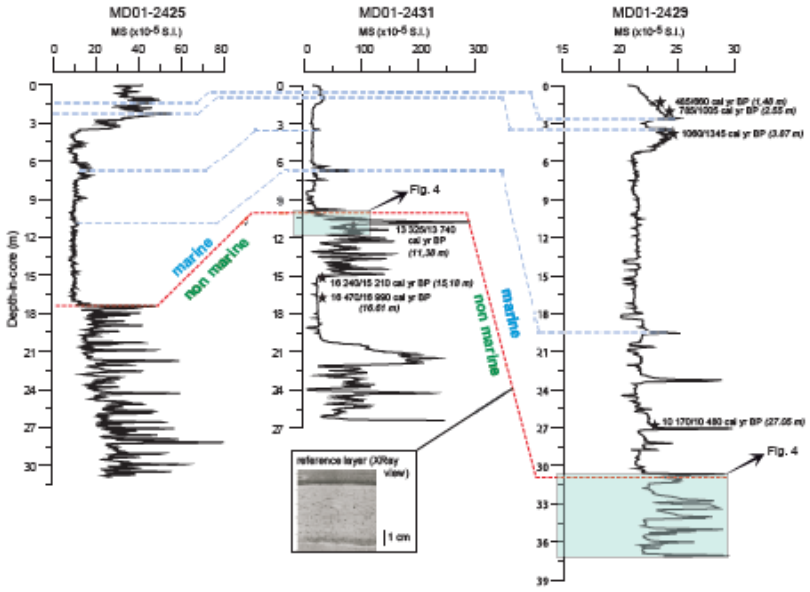

Figure 26. Chronostratigraphic correlations between the Çinarcik Basin (core MD01-2425) and the Central Basin (cores MD01-2429 and -2431) by Beck et al. (2015).

In terms of paleoseismicity, the results of Beck et al.(2015) only concern the pre-Holocene period. Regarding the thickness difference between cores MD01-2429 and MD01-2431 (3 times higher on the hanging wall), there is no drastic change at the nonmarine/marine limit. To explain the remaining thickness difference during the 13 kyr BP to present period, their hypothesis reveals two combined mechanisms: (1) the water vertical density profile led to more hyperpycnal distribution of gravity reworked sediments, and (2) coarse material strongly decreased due to change in weathering

condition. Considering a relatively low number of sedimentary events in the Central Basin with respect to Tekirdağ Basin, Drab et al. (2012) underlined a different explanation, including partial creeping along the central segment. For a longer period, they observed a similar difference between the Central Basin and Çınarcık Basin, with evidence of a specific behavior at the southern limit of the former. In the Central Basin, with up to 1.8 m normal slip values, added to local structural and seismological data, this archive can propose paleomagnitude values (MW) between 5.9 and 6.6.

The Holocene earthquake records from the Central Basin of the SoM have been presented by McHugh et al. (2014), who examined the physical and chemical composition of three 10 m-long cores recovered from the Central Basin (Fig. 27). In their study, they further explore the relation between sea floor fault ruptures and the generation of turbidity currents to better characterize fault segmentation and seismic hazards. For this purpose, submarine paleoseismology techniques are applied to study three cores and using multibeam bathymetry and chirp high resolution sub-bottom profiles. A chronology developed from radiocarbon and short-lived radioisotopes allowed the correlation of these T–H units to the historical record of earthquakes that goes back 2000 years. They found that the best location to recover the most complete sedimentation record is in the deepest part of a basin or "depocenter" where T–H units constitute ~80% of the sediments.

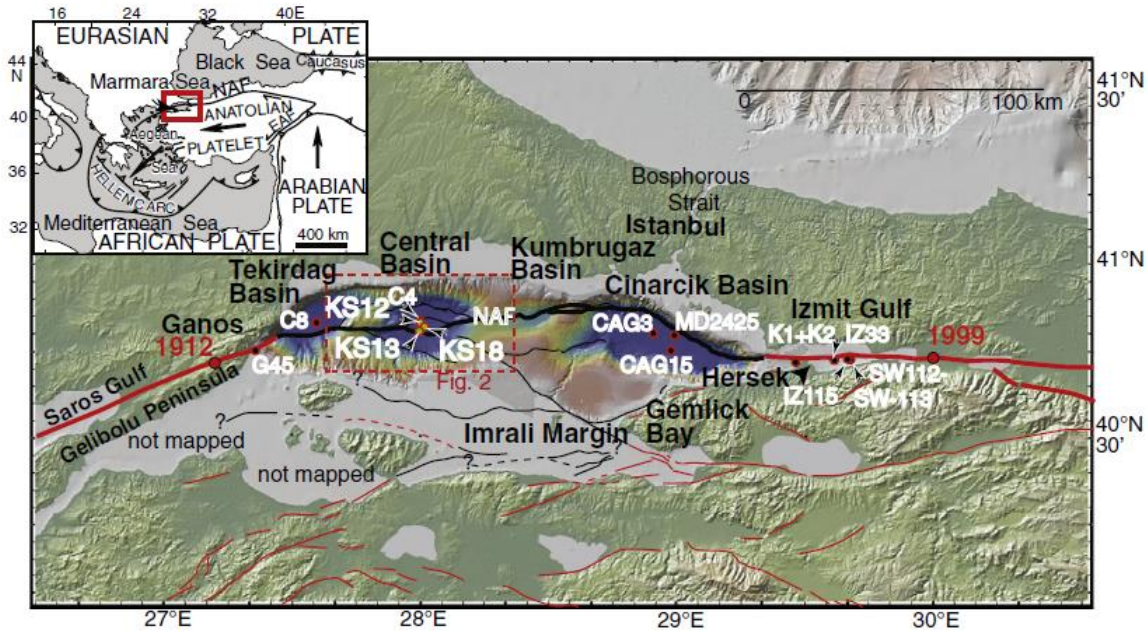

Figure 27. The North Anatolian Fault (NAF) system accommodates right lateralmotion between the Anatolia plate and Eurasia at 23 to 25mm per year (from McHugh et al., 2014). The main figure shows the NAF across northwest Turkey and the Marmara Sea. The red circles mark the epicentre locations for the 1999 Izmit and Duzce earthquakes to the east and 1912 Ganos earthquake to the west of Marmara Sea, respectively. The Marmara Sea is considered a seismic gap. The black and green circles mark the locations of cores from this study.

In Central Basin, the sedimentation history from cores KS13, 18 and 12 was used to identify turbidite–homogenite units (T–H units) by detailed analyses of the lithology, grain size, sedimentary structures and physical properties (McHugh et al., 2014; Figs. 28, 29 and 30). The detailed core analyses permit better quantification and documentation of the relation between sedimentation and earthquakes. In this study they mainly explored the relation between seafloor ruptures and the generation and deposition of T–H unit. These sedimentary deposits because of their particular fine structures, grain size variability and elemental composition are easier to date than mass-wasting deposits and can be better linked to seafloor ruptures along the North Anatolian Fault. Mchugh et al.

(2014) interpreted the core data within the context of the multibeam bathymetry and chirp sub-bottom profiles (Fig. 31). They established a good correlation between the three cores from Central Basin and historic earthquakes 1963 or 1964, 1343, 860, 740, 557 and 268. Except for 1963, the earthquakes being considered were Ms N 6.8 and are thought to have produced a seafloor rupture (Wells and Coppersmith, 1994) or a surface rupture onshore.

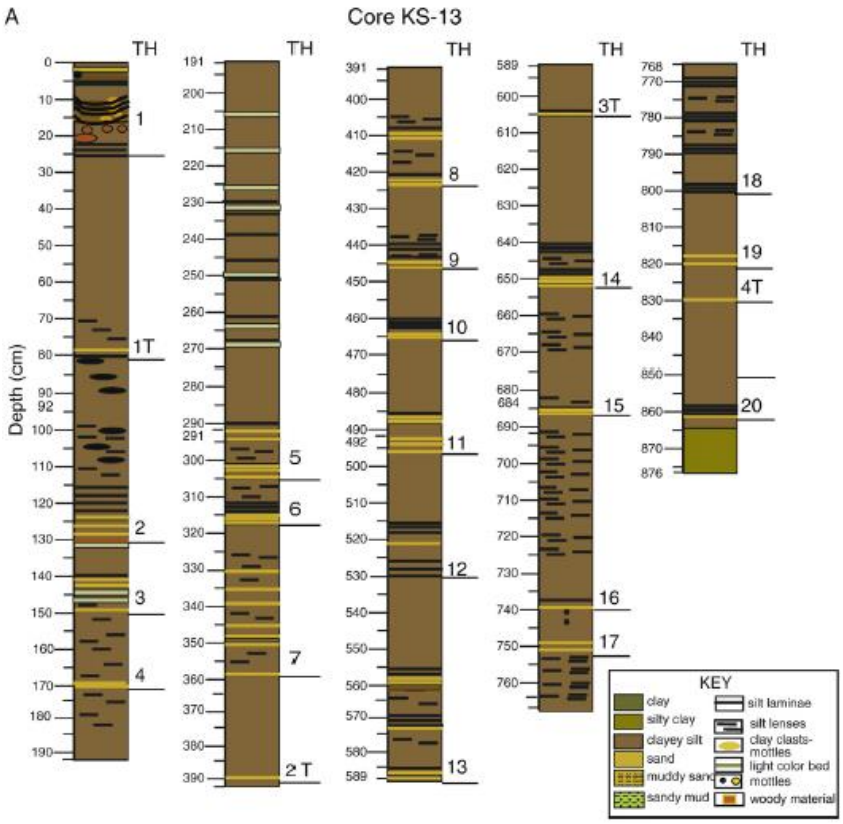

Figure 28. A. Lithostratigraphy and turbidite–homogenite (T–H) and turbidite (T) interpretation for Core KS-13 (McHugh et al., 2014).

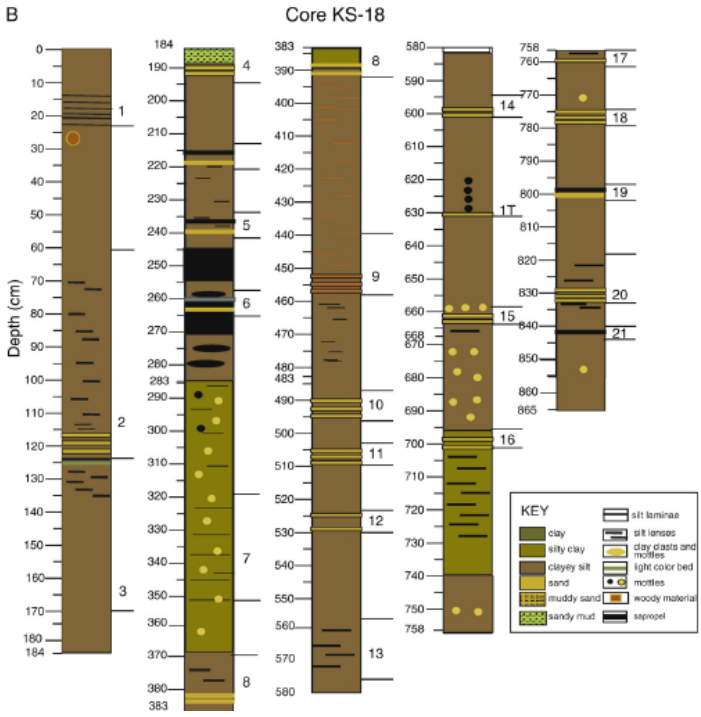

Figure. 29. A. Lithostratigraphy and turbidite–homogenite (T–H) and turbidite (T) interpretation for Core KS-18 (McHugh et al., 2014).

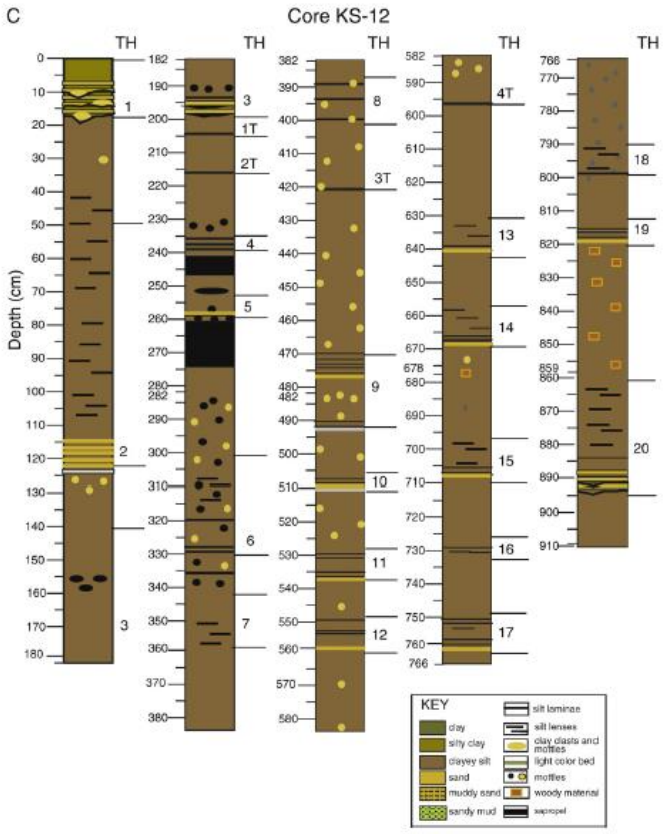

Figure. 30. A. Lithostratigraphy and turbidite–homogenite (T–H) and turbidite (T) interpretation for Core KS-12 (McHugh et al., 2014).

The results from McHugh et al. (2014) emphasize that the stratigraphic record of turbidite-homogenites can be linked to historical earthquakes and that the Holocene depocenters are the location from where to extract the most complete record. Core KS13 was recovered near a series of steep scarps of the NAF-N and contains several stratigraphic discontinuities most likely due to erosion and deformation along the NAF-N (Fig. 28). So when addressing the questions of how earthquake ruptures and sedimentation events correlate spatially in a basin, it is possible to say that there is a correlation. However, their findings from this study indicate that there is a remarkable correlation between the sedimentation record of a basin and the inferred approximate location of the historic earthquake rupture. A remarkable another conclusion of McHugh et al. (2014) that they support that the 1912 earthquake reached western Central Basin but did not rupture the fault across the entire basin as proposed by Armijo et al. (2005).

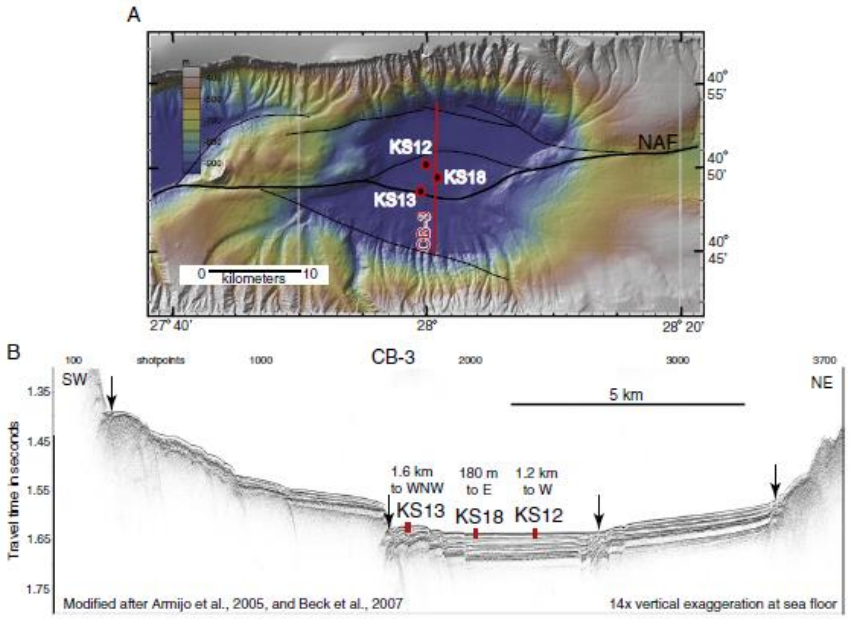

Figure 31. A. Multibeam bathymetry showing location of cores KS13, 18, and 12 and the trace of the several strands of the NAF (McHugh et al., 2014). The red line shows the location of high-resolution sub-bottom profile CB-3 across the Central Basin depocenter and core locations. B. Sub-bottom profile modified after Armijo et al. (2005) and Beck et al. (2007) showing the proximity of core KS13 to structures of the North Anatolia Fault

and cores KS18 and KS12 (recovered in the depocenter) from mainly undisturbed strata.

According to McHugh et al. (2014), seismically active transform basins such as in the Marmara Sea with frequent earthquakes are constantly shedding sediment and require high-sedimentation rates to preserve a complete "seismo-turbidite" in the stratigraphic record. Therefore, it is not surprising that there is a strong correlation between the location of the inferred historic epicentre and the sedimentary event in the adjacent basin. These basins are constantly shedding sediment (~every 300 years) and it is not expected that a basin distal to the inferred historical rupture will generate a large sedimentary event that is preserved in the stratigraphic record. The findings from McHugh et al. (2014) show a strong correlation between the locations of historical earthquakes and the preservation of turbidite–homogenite units in the basin adjacent to the inferred rupture.

The use of paleoseismological data to provide an accurate seismic risk assessment for the Çınarcık Basin has been recently well documented by Drab et al. (2015), using marine sediment cores (Fig. 32). In their study, a record of turbidites was obtained in two cores and used to reconstruct the earthquake history along the Çınarcık segment, a main branch of the NAF. The core Klg04 was collected from a berm north of the fault, and Core Klg03 was positioned in the Çınarcık basin, south of the fault. The cores were correlated using long-term geochemical variations in the sediment, and turbidites deposited simultaneously at both sites were then identified. They also used data from Core Klg06, located on the Western High, 100 km away from the Çınarcık basin (Fig. 33). The core spans the last 7 ky and does not contain a record of coarse-grained turbidites like the ones deposited in the basins of the Marmara Sea (Drab et al., 2015). In this study, a number of sedimentological investigations were performed to describe and characterize turbidites in the cores. Visual inspection shows that all sediment cores have mostly uniform silty-clay lithology with few sandy laminae containing shell fragments

(Fig. 33). These three cores were examined by using sedimentological and geochemical properties in order to make correlations of seismoturbidites on three sites (Fig. 34). Drab et al. (2015) also used east Mediterranean-scale changes in sedimentation to correlate the two records to a reference core located in a nonturbidite depositional environment. They then investigated the possible triggering mechanisms of the turbidites. Radiocarbon dating (^{14}C) combined with paleomagnetic data enabled them to construct an age model for the core Klg04 located in a berm in the Çınarcık fault scarp and to date turbidites over the last 1500 years.

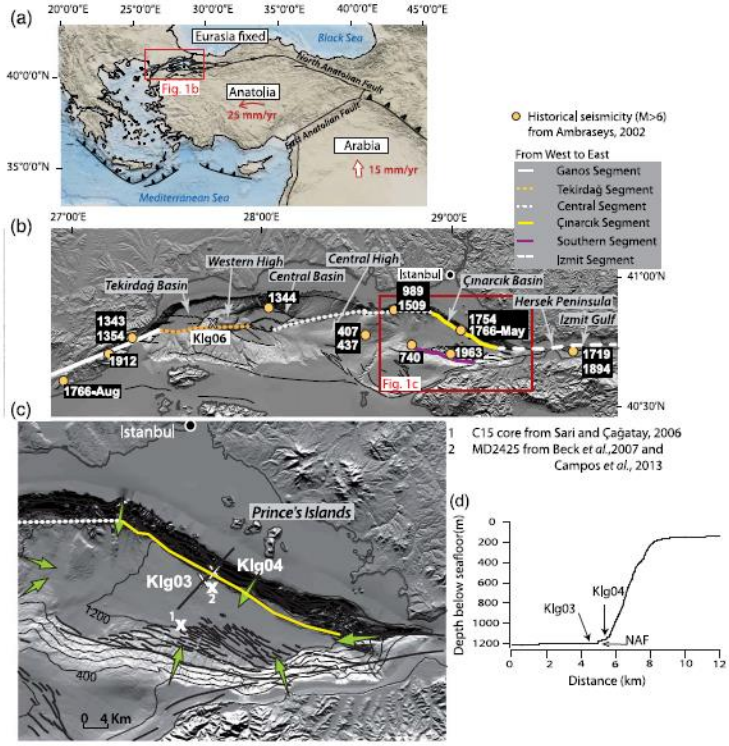

Figure 32. (a) Global geodynamic context of the Anatolian plate with Global Positioning System velocities from Reilinger et al. (2006). The location of the Marmara Sea (shown in [b]) is indicated with a box. (b) General tectonic map of the Marmara Sea, crossed by the North Anatolian fault (NAF). Basins, highs, and main segments of the fault are indicated from the west to the east with different lines, and their names are given in the gray box to the right. The study area (shown in [c]) is depicted with a box. Historical earthquakes located by Ambraseys (2002) are represented with rupture dates and dots. (c) The map of Çınarcık basin. Location of the two studied cores is represented with respect to the Çınarcık fault segment. Arrows show sediment paths for turbidite deposits

(Altınok et al., 2011). The line crossing the two cores represents the topographic profile presented in (d). White crosses represent the location of other published cores discussed in the study. (d) Topographic profile of the northern part of the Çınarcık basin.

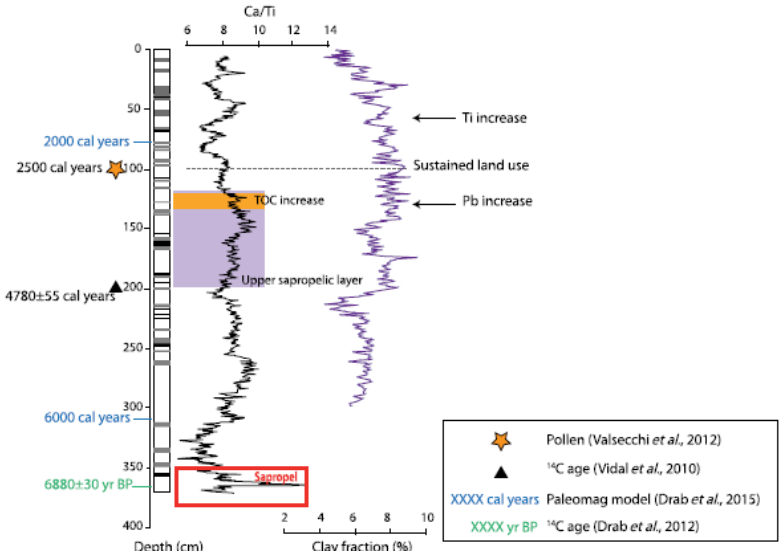

Figure 33. Summary of major Holocene sedimentation changes observed in core Klg06 with x-ray fluorescence (XRF), grain size, and total organic carbon content. Ages obtained from different studies (Vidal et al., 2010; Drab et al., 2012; Valsecchi et al., 2012; Drab et al., 2015) are indicated on the left side of the log.

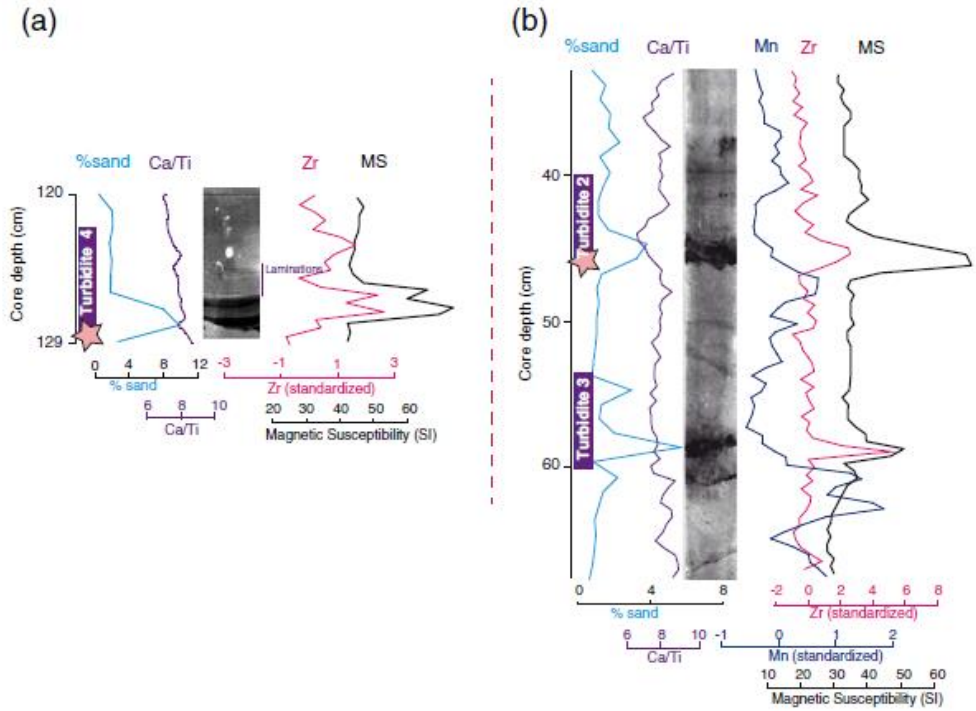

Figure 34. Typical examples of turbidites: grain size and geochemical (Ca=Ti, Mn, Zr, and magnetic susceptibility) signatures (Drab et al., 2015). Turbidites are composed of a

basal sand layer, an upper silt layer with frequent laminations, and an upper light-gray clayey layer. (a) X-ray imagery, grain size, and geochemical profiles of turbidite e4 at 120 cm depth in Klg03. (b) X-ray imagery, grain size,and geochemical profiles of turbidite e2 at 45 cm depth in Klg04. Manganese typically shows a peak just below turbidites.

Drab et al. (2015) used XRF data to identify other correlative changes in the Klg04 and Klg03 cores (Fig. 33). The correlation of Klg03 and Klg04 cores, excluding the coarse turbidites from the record has been well established (Fig. 32). The different proxies are used here to define similar time horizons between the cores Klg03 and Klg04. To assess the validity of their correlation, they additionally used NRM data as a different and independent proxy for core correlation. It represents changes in magnetic carrier and in the intensity of the magnetic field. The correlation between Klg03 and Klg04 based on geochemical proxies is in agreement with the magnetic data. Comparing turbidite-free sediment accumulation through time at the two sites (cores Klg04 and Klg03) provides some insights about major changes in sedimentation rates in the Çınarcık basin over the last 4000 years. Despite the differences in the turbidite occurrences, the two cores have similar accumulation rate curves and show identical major changes in sedimentation pattern.

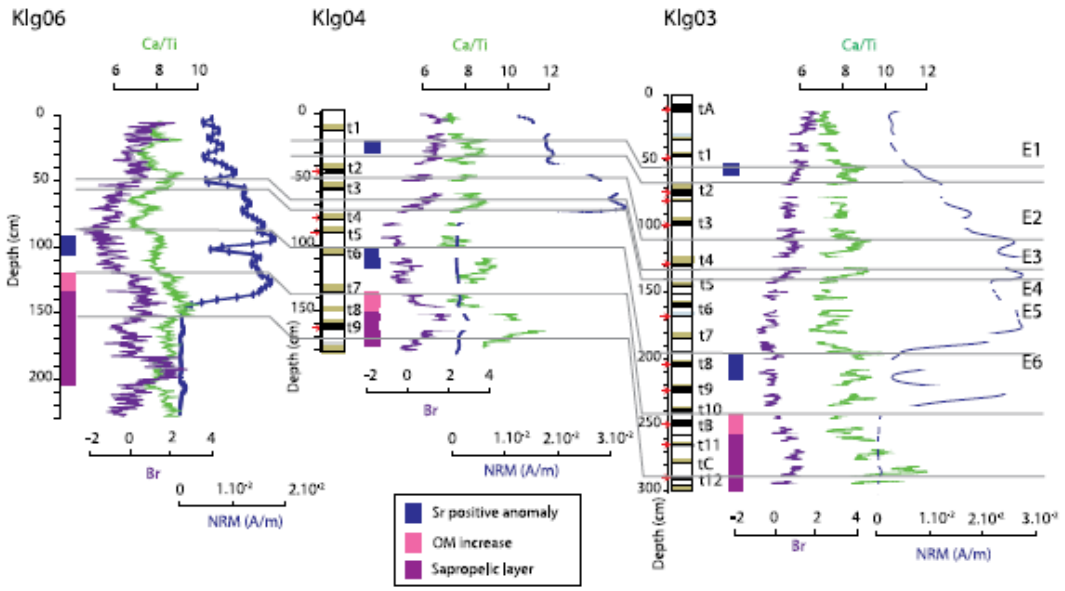

Figure 35. Correlation of cores Klg03, Klg04, and Klg06 according to XRF and natural remanent magnetization (NRM) measurements (Drab et al., 2015). NRM values decrease under the values of 1 × 10−2 A=m at 80 cm for Klg04, at 200 cm for Klg03, and 150 cm in Klg06 and are not considered reliable below these depths. The turbidite thicknesses have been deleted to solely correlate long-term environmental variations between the cores.

The arguments produced by Drab et al. (2015) indicate that turbidites deposited in the studied cores are seismically generated. However, the multiple sources for a turbidite deposits are linked to a series of catastrophic failures and turbidite currents triggered within perhaps minutes of each other. Such a phenomenon can uniquely be generated by earthquake shaking in the Marmara setting. Based on their sedimentological characteristics, large lateral extent, and synchronicity, Drab et al. (2015) concluded the turbidites deposited simultaneously in Klg03 and Klg04 are earthquake triggered. The original mass failure would come from the Çınarcık northern slope and must be related to rupture of the fault running at the slope base. They thus infered that these seismoturbidites have been triggered by large earthquakes along the northern Çınarcık fault segment.

The establishing criteria for identification of seismoturbidites and determination of the earthquake records in the İzmit Gulf has been documented by Çağatay et al. (2012). Apart from the subbasins of the SoM, the 17 August 1999 İzmit earthquake (Mw=7.4) ruptured the entire 55-km length of the İzmit Gulf along the northern branch of the NAF (Polonia et al., 2004; Cormier et al., 2006; Gasperini et al., 2011). In this study, they present a detailed analysis of the 1999 İzmit and older earthquake records extending back to 2400 a BP in sediment cores obtained from the 210 m deep depocentre of the Karamürsel Basin in the central part of the İzmit Gulf (Fig. 36). The cores were analysed to characterise the mass-flow units using grain-size analysis, physical properties, and dated by radionuclide and radiocarbon analyses. The high variability of geochemical and physical properties (density and magnetic susceptibility, MS) of the mass-flow units probably indicates different sediment sources. The depositional features, together with confident matching of the ages of THUs with historical records, strongly suggest that they have been triggered by earthquakes on the İzmit Gulf segment of the NAF.

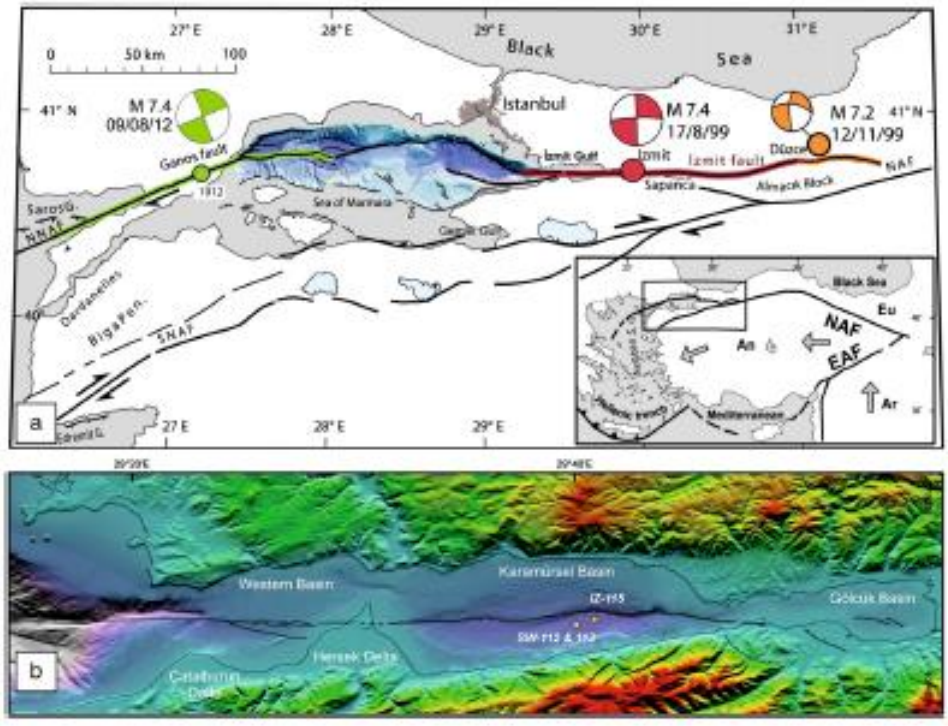

Figure. 36. (a) Tectonic map of the Marmara region (modified from Uçarkuş et al., 2011) including the EM300 bathymetry of the Sea of Marmara (Le Pichon et al., 2001), showing the active faults (Armijo et al., 2002) and surface ruptures of the 1999 İzmit (red), 1999 Düzce (orange) and 1912 Şarköy (Ganos) (green) earthquakes (Barka et al., 2002) with focal mechanism solutions from Harvard CMT. Inset map presents the tectonics of the eastern Mediterranean with arrows showing the movement of Arabia (Ar) and Anatolia (An) relative to Eurasia (Eu). (b) The bathymetric map of the Gulf of İzmit (Polonia et al., 2004; Bortoluzzi et al., 2005; Kurt and Yücesoy, 2009; Uçarkuş et al., 2011) showing the location of the studied sediment/water interface Cores SW-112 and 113 and gravity Core IZ-115.

Careful dating of seismoturbidites on different segments of the NAFZ can provide data on re-occurrence time and the age of the last event, which are important in probabilistic earthquake risk assessment. The sedimentary section deposited in the last 2400 a in the Karamürsel Basin of the İzmit Gulf provides eight earthquake records along the İzmit segment of the NAF, giving an average recurrence time of 300 yrs (Çağatay et al., 2012). This result is in agreement with GPS rates (2.4 cm/yr; McClusky et al., 2000) and the lateral offset of the 1999 İzmit earthquake (4.5–5 m). However, the time interval between consecutive earthquakes is highly variable, ranging between 90 and 695. Another important conclusion from the foregoing discussion on matching the sedimentary and historical earthquake records is that the epicentre allocation of some earthquakes (865 AD) close to İstanbul may be incorrect, and that the effect of other major events (740 AD and 1509) may have extended into the İzmit Gulf. Based on detailed sedimentological and geochemical analysis on the core sediments, Çağatay et al. (2012) presented remarkable conclusions regarding to physical and chemical conditions of water column during deposition of seismoturbidites. Their findings reveal that the bottom coarse layers in seismoturbidites are commonly graded and laminated with local bi-directional foresets indicating water-column oscillations (i.e., seiches) and deposition

from turbidity currents reflecting or deflecting from the opposite slopes of the Karamürsel Basin. The mass transport processes, resuspension and deposition/redeposition generate transient redox conditions, with the formation of a new redox front after the formation of each mass-flow unit (Chaillou et al., 2008). Based on XRF analysis, high Mn enrichment and depletion were observed in the sediment cores above and below the base of each turbidite-homogenite layer, respectively.

During the large earthquakes occurring on the North Anatolian Fault, numerous submarine mass movements have occurred and the most recent turbidites in the basins of the SoM have been related to historical earthquakes (Zitter et al., 2012; Grall et al., 2014). Grall et al. (2014) proposed the relationship between mass wasting and sea-level changes over the last 400–500 ka that is evaluated using high resolution seismic records (Fig. 37). The Mass-Transport Deposits (MTDs) related to sea-level oscillations and marine/lacustrine transitions have been characterized, and the possible MTDs trigger processes discussed in their study (Grall et al., 2014). Detailed analysis, using a 3D high-resolution seismic dataset, of stratigraphy over the last 500 ka, within a ponded basin of the Western High, shows that intervals of draped sedimentary reflectors alternate with onlap sequences that followed episodes of rapid sea-level rise, with a periodicity of approximately 100,000 years (corresponding to glacial cycles). Mass Transport Deposits (MTDs) occur within the onlapping sequences. Mass-wasting occurrence and size increased during the end of the glaciation period which may be attributed to thermal destabilization of gas hydrate or variations in sediment supply (Zitter et al., 2012).

Grall et al. (2014) remarked that the cyclic occurrence of MTDs observed in a ponded basin of the Western High in the SoM could correlate with glacial-interglacial sequences. Despite that slope instabilities are presumably triggered by earthquakes, their

size and/or frequency appears to be modulated by glacio-eustatic oscillations and the lacustrine/marine transitions associated to them. The swelling of clays in marine sediments under low salinity brackish water can promote slope instability after marine to lacustrine transitions, and may be one factor contributing to long-term cyclicity of slope instability occurrence in the Sea of Marmara.

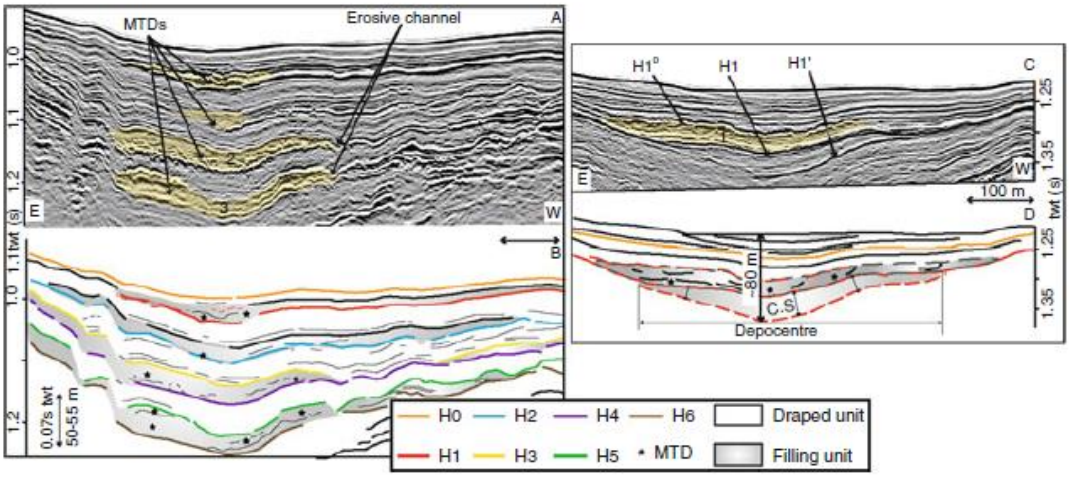

*Figure. 37. (**a**) Seismic section across the northern edge of the Eastern Fault-Zone Basin (Grall et al., 2014). MTDs are highlighted in yellow, and numbers 1, 2, 3 refer to the three most remarkable MTDs discussed in the text. (**b**) Line drawing of the seismic section above. Horizon numbers mentioned increase from top to bottom. Stratigraphic sequences contain one basin filling unit (in grey) in which MTDs occurred (indicate by black stars), and one draped section (in white). The four main stratigraphic sequences in this characteristic seismic section have a thickness of around 65–75 ms twt, which represent around 50–63 m (P-wave velocity ranges between 1,515 (above H1) and 1,660 m/s (between H6 and H4), within the sediments, Thomas et al., 2012). (**c**) Seismic section across the Eastern Fault-Zone Basin, showing details of the first stratigraphic sequence below the seafloor. (**d**) Line drawing of the seismic section above. The filling unit contains a condensed section (H10–H1) on which MTDs occurred (between H1 and H10).*

The slopes of the Sea of Marmara, that have been intensively surveyed since the 1999 Izmit–Kocaeli earthquake, display numerous morphological signs of recent mass wasting processes (Görür and Çağatay, 2010; Özeren et al., 2010). Zitter et al. (2012)

gave an overview of the distribution, extent and timing of recent mass wasting features; then, based on the results of an analysis carried out over a number of different cases in different sectors of the SoM, they discussed the possible influence of tectonics and sea-level changes on triggering instabilities. All submarine mass wasting features identified on the seafloor of the SoM in this study. They mapped mass wasting features in the Sea of Marmara that demonstrates the widespread occurrence of slope instabilities. The Sea of Marmara indeed presents favorable conditions for submarine mass movement, with high sedimentation rates, dominated by silico-clastic deposits. A diversity of mass wasting processes occurs as mainly landslides, mass flows and creep. Zitter et al. (2012) can distinguish gravity slides related to erosional processes within the canyons, initiated from the head walls and the incised channels of the canyons from wider unstable slopes that appear associated with transtensional crustal deformation evidenced from microseismicity. Following the marine/lacustrine transition depth to the west, Zitter et al. (2012) observed large debris flow that is characterized by the transparent acoustic reflection. This remarkable event has been interpreted to occur during the lacustrine to marine transition or shortly afterwards at ca. 14 cal. Ka BP (Zitter et al., 2012). This finding seems to be well consistent with the result of Eriş et al. (2012) from the Çınarcık Basin.

Comparision of earthquake sedimentary records in subbasins of the SoM

Regional and localized correlations of earthquake sedimentary records have been established in various studies in the SoM (Beck et al., 2015; Campos et al., 2013; Drab et al., 2012, 2015; Eriş et al., 2012; McHugh et al., 2014). The main aim for localized comparisions of seismoturbidites obtained from the different cores in the same basin is an occurrence of coseismic offsets through coeval specific events, and therefore, it allows

estimating the vertical component of coseismic displacement of the each segment of the NAFZ. The main purpose for regional correlations of dated specific earthquake record is to demonstrate the earthquake origin of a sedimentary "event'' that provide us to determine segmentation of the NAFZ.

Eriş et al. (2012) attempt to correlate possible major mass flow events that occurred in the sub-basins of the SoM during the Late Pleistocene to Holocene using high resolution seismic and core data. This correlation suggests that turbidites were generated by historic earthquakes along the NAF. However, the effects of tectonic activity are evident from the presence of seismically transparent layers in the seismic data from the other subbasins of the SoM. In this study, the high-resolution seismic images from the other subbasins (Tekirdağ and Central basins) allowed them to investigate the same seismic event (Figs. 4, 5 and 9). For example, in the Tekirdağ Basin, the mass-wasting deposit as a result of this major seismic event can be imaged as a thick, acoustically-transparent sedimentary unit. The sedimentary record of this synchronous seismic event from the Çınarcık Basin is also shown both by seismic and core data (Fig. 9). This major transparent layer can be confidently correlated with the homogenite layer described by Beck et al. (2007) from the Central Basin. The wide lateral extent of the 'homogenite layer' across these three subbasins of the SoM can be attributed to a regional seismic event rather than a local one. This homogenite layer has been estimated to be generated at the end of the lacustrine phase of the SoM, while it is overlain by 12.3 cal ka BP dated Q1 unconformity surface in the profiles.

Beck et al. (2015) focused on two cored sites on both sides (cores MD01-2429 and MD01-2431) of the southern limit of the "inner" Central Basin. In order to extract a paleoseismic record through homogenite-turbidite events, Beck et al. (2015) checked (1)

a regional correlation between the Central and Çinarcik basins (MD01-2425, -2429, and -2431; see also Eriş et al., 2012), and (2) a more localized correlation on both sides of the active scarp bounding the inner Central Basin on its southwestern side. However, they established precise correlations (especially event-by-event) as previously done by Drab et al. (2012) for the 2 late millennia using shorter gravity cores. This proposed event-by-event correlation was strengthened by (i) precise delimitation of the hemipelagic intervals, with same thicknesses, and (ii) similarities of subdivisions within HmTu composite layers. For a 2 kyr long interval, 11 events could be precisely correlated on both sides of the Central Basin's southwestern scarp. For each of them, based on the specific depositional process, the thickness difference between the two sites (MD01-2429 and MD01-2431) was considered as a direct estimation of the vertical component of a coeval coseismic offset. The homogenite (upper) component accounts for the major part of the thickness difference (ranging from 36 to 144 cm). In the Central Basin, the discovery and the multicriteria characterization of a specific layer allowed defining a "reference" thin layer which is independent from any earthquake-/landslide-triggered sedimentary event and was also recognized in Çinarcik Basin's long core (MD01-2425), rather indicating a general paleoenvironmental event (Beck et al., 2015).

Investigations of the earthquake sedimentary records from the core sediments in the Çınarcık Basin by Drab et al. (2015) provided comparision between two coring sites and also correlation with findings from the other subbasins in the SoM. The seismoturbidites from the different coring sites have been used to constrain the history of earthquakes rupturing across a given depocenter (McHugh et al., 2014; Drab et al., 2012). Their study shows that marine sediment cores can be used to constrain paleoruptures of the NAF segment located just south of Istanbul. In the inner part of the Central Basin, the core data

shows eleven major turbidites, which display a greater diversity in their geochemistry and textural pattern (Drab et al., 2012). The observed diversity may reflect a larger variability in the emplacement and in the sources of turbidites in the inner Central Basin compared to the Tekirdağ Basin. The correlation of the Klg02 to Klg08 cores across the whole Marmara Sea was done by combining granulometry, Ca/Ti ratio, Ti, Pb, Br and Sr intensities with the obtained chronological data. Marked geochemical and granulometric variations are used as chronological markers and are tentatively interpreted as global changes in the sedimentation pattern of the Marmara Sea related to anthropogenic disturbances. The inner Central Basin (Klg02) located between the Tekirdağ and the Central faults can also record mass wasting events synchronous with the Tekirdağ Basin. According to Drab et al. (2012), another noticeable paleoseismological result is the relatively low number of turbiditic events recorded in the Central Basin, which could record earthquakes rupturing in the Tekirdağ and Central Segments. Their study indicated that the last possibility would be a less frequent earthquake rupture of the Central Segment that would be related to partial creep along that specific segment. A partial creep would mean a lower recurrence rate and maximum magnitude on the Central Segment than on the other NAF segments.

Drab et al. (2012) documented the 1912 event based on an age model constructed from excess ^{210}Pb in two cores in Tekirdag Basin and the Central high, respectively, and one core from Central Basin. The sedimentary imprint of same earthquake in the Central Basin suggests that the rupture of the Tekirdağ Segment can generate turbidites in the Central Basin (Drab et al., 2012). This implies that the two different depocenters of the Marmara Sea, which are the Tekirdağ and the Central Basins, may have the potential to record the same large magnitude earthquake. Based on the seismic profiles, turbidites in

the Central Basin have thus significant lateral extension (Eriş et al., 2012; Beck et al., 2015). The inner Central Basin (Klg02) located between the Tekirdağ and the Central faults can also record mass wasting events synchronous with the Tekirdağ Basin (Drab et al., 2012). The relatively low number of turbidites documented in the Central Basin compared to the Tekirdağ Basin might be linked to ruptures in close sequence on the Tekirdağ and Central Segments, like in 1766 (Pondard et al., 2007) or to creeping along the Central Segment.

McHugh et al. (2014) examined the core data from the Tekirdağ, Central and Çınarcık basins in order to document earthquake records that were possibly triggered by NAFZ along the SoM. Their results show that there is a remarkable correlation between the inferred location of the historic earthquake rupture and the seismo-turbidite record in the basin adjacent to the fault rupture. Their results when compared to findings from other transform basins in Marmara Sea reveal a very good correlation between T–H units and historic ruptures. Most importantly, there is a strong correlation between the inferred locations of historical earthquakes and the preservation of turbidite–homogenite units in the basin adjacent to the inferred rupture. Seismically active transform basins such as in the Marmara Sea with frequent earthquakes are constantly shedding sediment and require high-sedimentation rates to preserve a complete "seismo-turbidite" in the stratigraphic record. A good correlation was obtained for T–H units in Central Basin and historic earthquakes that occurred in 1963 or 1964, 1343, 860, 740, 557 and 268 (McHugh et al., 2014). Except for 1963, the earthquakes being considered were Ms N 6.8 and are thought to have produced a seafloor rupture (Wells and Coppersmith, 1994) or a surface rupture onshore. Amain requirement used for the correlation of the T–H in between cores was that at least two of the cores had comparable radiocarbon ages. McHugh et al. (2014)

emphasize that the stratigraphic record of T–Hs can be linked to historical earthquakes and that the Holocene depocenters are the location from where to extract the most complete record. Core KS13 from the Central Basin was recovered near a series of steep scarps of the NAF-N and contains several stratigraphic discontinuities most likely due to erosion and deformation along the NAF-N. So when addressing the questions of how earthquake ruptures and sedimentation events correlate spatially in a basin, it is possible to say that there is a correlation.

The ages calculated by Drab et al. (2012) for the 1766b and 1343 and/or 1354 events from cores in Tekirdağ Basin were obtained from shells and bulk sediment and are too old and not reliable to document these earthquakes (as per Drab et al., 2012). Based on the facts from McHugh et al. (2014), the 1343 rupture did not likely extend into Tekirdağ Basin and the Ganos region. The proximity of this T–H to the 1063 rupture is consistent with historic accounts of large shocks from the towns of Tekirdağ to Erdek (southernwestern Marmara Sea shore), and damage in towns near western Marmara Sea (Ambraseys, 2009). Indeed, McHugh et al. (2014) did not find evidence of the 1063 earthquake in Central Basin. 1063 rupture must have been very close to the NAF in Tekirdağ Basin possibly extending from onshore and through Tekirdağ Basin. This indicates that the 740 AD event extended from Izmit Gulf to the Central Basin suggesting that this earthquake ruptured at least 170 kmalong theNAF-N, including several fault segments. It would have had a larger magnitude than M7.1 as proposed by Ambraseys (2002a) (Wells and Coppersmith, 1994). The rupture of the 1999 Izmit earthquake did not reach Çınarcik Basin (Cormier et al., 2006; Gasperini et al., 2011) and this is consistent with Drab's (2012) findings of a very small sedimentary disturbance.

Correlation of seismic events with historical data and earthquake reoccurrence time for different subbasins

Seismic hazard assessment is a challenging issue for modern societies. A key parameter to be estimated is the recurrence interval of damaging earthquakes, this requires the establishment of earthquake records long enough to be relevant, *i.e.* far longer than historical observations. However, the recurrence interval of strong earthquakes often exceeds the time span covered by instrumental and historical records in moderately active seismo-tectonic regions. Hence, extending time series of seismic events is a key issue for understanding regional seismicity and for assessing the earthquake-hazard potential of such regions (e.g. Strasser et al., 2006; Avşar et al., 2014).

A well-dated and quantitative earthquake history of SoM is required for the assessment of long-term probabilistic seismic hazard related to NAFZ. In the Sea of Marmara, different investigations have highlighted the earthquake records longer than historical observations. Radionuclide and radiocarbon dated seismoturbidite layers in different basins of the SoM can be confidently correlated with historical earthquake records (McHugh et al., 2006, 2014; Beck et al., 2007, 2015; Eriş et al., 2012; Çağatay et al., 2012; Drab et al., 2012, 2015). The ^{210}Pb data of the core sediments provide a chronology of the most recent sedimentary events, such as seismoturbidites triggered by the 1912 M =7.4 Mürefte earthquake. The most recent turbidites in the Tekirdağ Basin and in the Western High have been interpreted in Klg05 and Klg08 cores (Drab et al., 2012). Seismoturbidite layers have two basal sandy layers, which are characteristic of turbidites deposited at the Klg05 site in the Tekirdağ Basin. The inner Central Basin (Klg02) located between the Tekirdağ and the Central faults can also record mass wasting events synchronous with the Tekirdağ Basin. The first example is the 1912 disturbances triggered by the rupture of the Tekirdağ fault. The latter implies massive slope failures,

both in Tekirdağ and Central Basins. It might have been triggered by the Tekirdağ fault rupture alone, but was most probably triggered by the quasisynchronous rupture of the Tekirdağ and Central faults. The earthquake has also left a sedimentary imprint in the Central Basin, which suggests that the rupture of the Tekirdağ Segment can generate turbidites in the Central Basin. This implies that the two different depocenters of the Marmara Sea, which are the Tekirdağ and the Central Basins, may have the potential to record the same large magnitude earthquake. The sedimentary cores studied by Drab et al. (2012) provide a paleoseismological record of the Tekirdağ fault ruptures. The 1912 Mürefte earthquake (event 1) was recorded in the Tekirdağ Basin and in the Western High, as well as in Central Basin where it has a faint expression. Considering the ^{14}C age of 2185 yr BP below event 6 in core Klg05 with the reservoir correction of 340–460 yr proposed by McHugh et al. (2006), the mean recurrence time of events along the Tekirdağ fault would be about 300 yr. In their study, the sedimentary earthquake imprints can be well correlated with 1766, 1354 or 1343, 1063, 557 or 437.

According to Drab et al. (2015), the turbidite record deposited in a minor push-up structure along the Çınarcık fault places some new constraints regarding past ruptures of the Çınarcık Fault. They combine the historical catalog with the proposed age model to reconstruct an history of ruptures along the Çınarcık fault (Fig. 38). Core Klg04, located on the berm in the northern fault margin of the Çınarcık Basin, likely records earthquakes rupturing the Çınarcık fault, whereas core Klg03 may record earthquakes occurring on other faults and highlights the different sensitivity of both sites to earthquakes. Drab et al. (2015) estimated the timing of the first six sedimentary events using radiocarbon dating, radionuclides, and paleomagnetism measurements (Fig. 38). The first earthquake-related turbidite recorded in the cores corresponds to the 1894 C.E. earthquake. The

seismoturbidite layer occurred between 1364 and 1511 C.E and that is probably related to the 1509 C.E. historical earthquake. Another event was dated 1268–1360 C.E. and was likely generated by the 1344 C.E. earthquake. The integration of results in Drab et al. (2015) proposes a coherent scenario of past ruptures along the Çınarcık fault, which can be used for seismic-hazard assessment. Indeed, their observations help relocate some earthquakes for which the rupture segment is still under debate. They suggest that the 1766 C.E. earthquake did not occur along the Çınarcık fault, but that the 1344 C.E. earthquake was likely related to its activation.

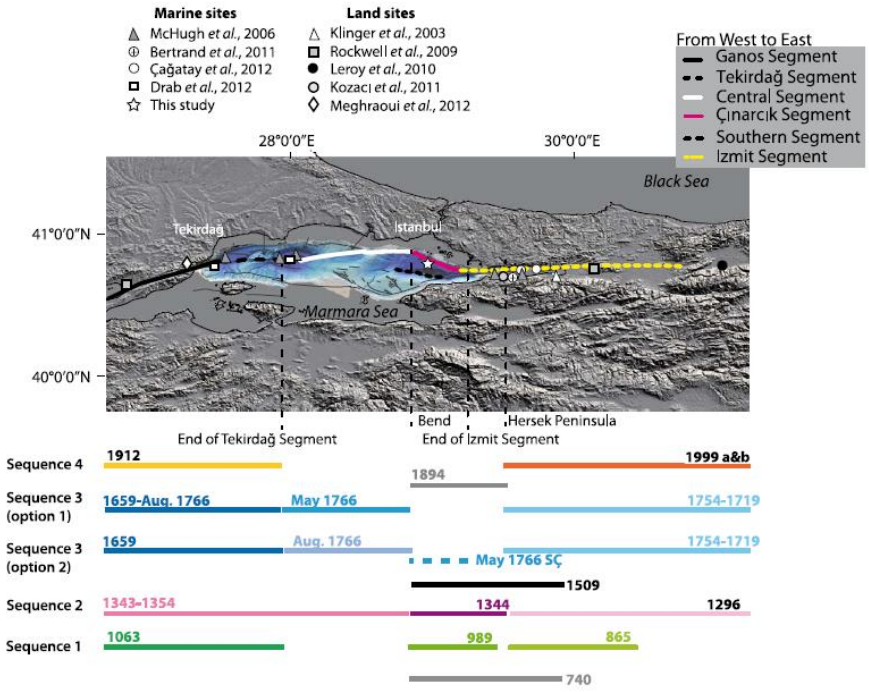

Figure 38. Proposed rupture scenario for Mw >6:8 earthquakes in the Marmara Sea between C.E. 740 and 1999 (Drab et al., 2015). Four sequences are observed, but only three are complete. The twentieth century westward propagation had not yet ruptured the eastern Marmara Sea. The scenario is compatible with a recent Coulomb stress analysis (Pondard et al., 2007) and description of damage (Ambraseys, 2002). Different shapes represent onland and submarine paleoseismological investigations of NAF ruptures in and around the Marmara Sea.

The detailed core analyses by McHugh et al. (2014) permit better quantification and documentation of the relation between sedimentation and earthquakes. A good

correlation has been established between the three cores from Central Basin for T–Hs 1–6 and historic earthquakes 1963 or 1964, 1343, 860, 740, 557 and 268 (Table 4). The radiocarbon ages obtained in the Central Basin cores extended the T–H record back to ~6000 years BP. The recurrence intervals along the central Marmara segment of the North Anatolia Fault are 569, 280, 203, 120 183, and 289 implying an averaged recurrence of ~274 years (McHugh et al., 2014). For the Istanbul segment of the fault, McHugh et al. (2014) documented the 1509 and 1766a historic ruptures, and for the western Izmit segment the 180, 268, 358, 740, 860, 1296, 1509, 1766a, 1894 and 1999 earthquakes with an average recurrence of ~200 years (also McHugh et al., 2006; Çağatay et al., 2012; Drab et al., 2012). In their study, a good correlation was obtained for T–H units in Central Basin and historic earthquakes that occurred in 1963 or 1964, 1343, 860, 740, 557 and 268. Overall, the sedimentation record for the Marmara Sea basins suggests that there is a gap in the earthquakes in Central Basin since 1343. Their results indicate that earthquake clustering (1343, 1344, 1354) could have produced several metres of slip and diminished strain accumulation along the NAF in Central Basin. McHugh et al. (2014) concluded that the 740 AD earthquake could have ruptured multiple segments of the NSF from Izmit Gulf to Central Basin. Based on this and previous studies of seafloor ruptures in Marmara Sea a tentative recurrence interval can be established for the NAF from Ganos to Çınarcık Basin. The results obtained from Central Basin, the 1912 rupture documented in a “ponded basin”, 40 km east of the inferred Ganos epicentral region and in Tekirdağ Basin, and the 1063 historic earthquake documented in Tekirdağ Basin provide a record for historic earthquakes for the NAF-N in 1912, 1343, 1063, 860, 740, 557, and 268 (Fig. 24; Table 4; McHugh et al., 2006; Drab et al., 2012).

Table 4. Age in years AD and BC for Cores KS13, 18, and 12. Interval (cm) fromwhere the sampleswere dated, T–Hunit numbers adjusted for the missing stratigraphic record, historical earthquake, and recurrence interval. disc = discontinuity (McHugh et al., 2014).

Core KS-13	Int. cm	T–H	KS-18	Int. cm	T–H	KS-12	Int. cm	T–H	Historic eq.	Int. yrs
		1			1			1	1963 or 1964	
1965 AD	25		1965 AD	28		1965 AD	20			620
		2			2			2	1343	
disc.						910 AD	122			483
		no 3	disc.		no 3			3	860	
			760 AD	124						120
		no 4			4	disc.		no 4	740	
505 AD	123		610 AD	192						183
		5			5			no 5	557	
										298
		6			6			6	268	
						290 AD	198			
		7			7			7		
		8			8			8		
			835 BC	392						1125
1340 BC	317									
		9			9			9		
			1490 BC	460		1425 BC	478			655
		10			10			10		
1690 BC	355		1670 BC	500		1630 BC	570			–200
		11			11			11		
		12			12			12		
		13			13			13		
					14			14		
			1772 BC	605		2 σ –1747 BC	642			–50
disc.										
					15			15		
					16			16		
					17			17		
					18			18		
2960 BC	497		2850 BC	780						–300
		19			19			19		
		20			20			20		
		21			21					
		22–26								
3685 BC	840									

In Çınarcık Basin, in terms of paleoseismicity, the remarkable results from the Central Basin by Beck et al. (2015) only concern the pre-Holocene period. The inferred offsets were separated by variable time intervals (100–550 yr); if taking into account the 11 events, a mean 180 yr interval can be deduced. The time distribution is in agreement with previously published paleoseismic results based on sedimentary records in the same area (Beck et al., 2007; Drab et al., 2012). This difference is also mentioned by Drab et al. (2012) for the last 2.5 kyr BP (marine section); based on a precise chronology on short

piston cores, these authors could propose several event-by-event correlations and their attribution to historical earthquakes.

The earthquake records in the Karamürsel Basin of the İzmit Gulf in the SoM have been documented as Turbidite-Homogenite (THU) by Çağatay et al. (2012). The radionuclide data, together with a post-bomb AMS ^{14}C age, support the sedimentological evidence that THU-1 in the upper part of the studied core is indeed a recently deposited unit triggered by the 17 August 1999 Mw=7.4 İzmit earthquake. In their study, below the 1999 İzmit earthquake record (THU-1), eight mass-flow units were identified in the sedimentary column and seven of them were dated by AMS ^{14}C method. These THUs are correlated with the historical earthquakes of 1509 AD (Ms=7.2), 1296 AD (I=VII), 865 AD, 740 AD (I=VIII), 358 AD (I=IX), 268 AD and 427 BC. Their observations suggest that the epicentre assignments of some historical earthquakes may be incorrect: the 865 AD and 740 AD earthquakes located close to İstanbul on the basis of historical reports could have had effects extending well into the İzmit Gulf; others assigned to İzmit area (e.g., the 1719 earthquake) may have their epicentre further east of the İzmit Gulf. According to Çağatay et al. (2012), the sedimentary records of eight major earthquakes during the last 2400 a provide an average recurrence time of 300 a that is in agreement with historical records, GPS measurements and the lateral offset of the earthquake ruptures in the SoM. However, the intervals between the consecutive events are highly variable, ranging from 90 to 695 a.

In summary, the sedimentary records measured over more than 5000 yrs provide average earthquake recurrence time between 220 and 300 yrs for the various segments of northern branch, and 1000 yrs for the middle NAF branch in the Gemlik Gulf (Fig. 38). These results are compatible with GPS velocities and geological slip rates. However, the

intervals between two consecutive events vary widely between 90 to 1500 years for the different northern NAF segments. The last earthquake event recorded in the Gölcük and Karamürsel basins is the 1999; on Prince Islands segment in the Çınarcık Basin the1794; in the Central High and Central Basin the 1963; in the Tekirdağ Basin and Western High the 1912; and in the Gemlik Gulf the 1855 earthquakes. The western High and Central Basin records suggest that the 1912 earthquake rupture is unlikely to have reached beyond Western High into the Central Basin. The only earthquake recorded on the sediment covered Central High segment for the last 15 ka is a faint, far-field expression of the 1963 event having an assigned epicentre in the southern Çınarcık Basin. This suggests that the Central High segment SW of Istanbul has been creeping, and that the rupture of the 1963 earthquake may have extended from the southern Cinarcik Basin to the Central High.

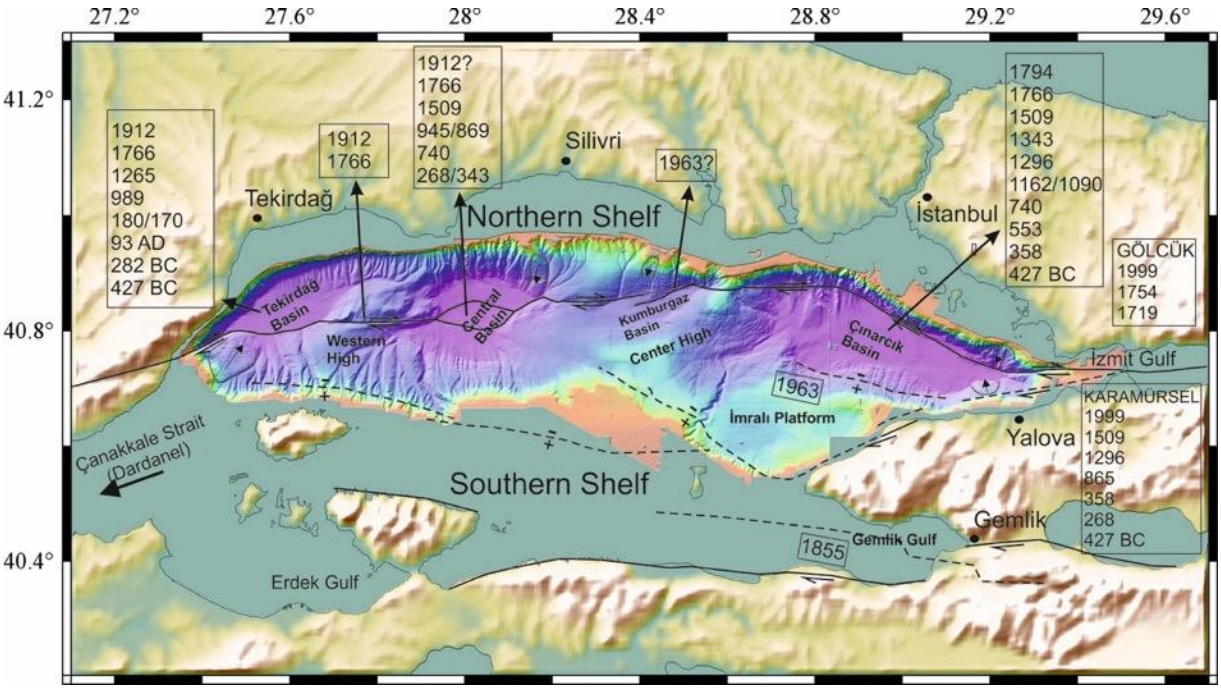

Figure 38. The multi-beam bathymetry map showing historical earthquakes recorded by different sediment cores along the various segments of northern branch that were documented by various studies in the SoM (Çağatay et al., 2012; Drab et al., 2012, 2015; McHugh et al., 2014; Beck et al., 2015).

Depositional Processes of Seismoturbidites

The triggering mechanisms and the consequent depositional processes of seismoturbidites have been extensively discussed by various researches with the main purpose of relating them to either transporting mechanism and seismic source along the SoM (Beck et al., 2007, 2015; Çağatay et al., 2012; Eriş et al., 2012; Drab et al., 2015; McHugh et al., 2014). All these investigations have been based on multi-proxies including core sedimentology, geochemistry and geophysical analysis of the sediments and basin itself. The most remarkable conclusions have been provided from core studies in the Çınarcık Basin (Eriş et al., 2012; Beck et al., 2015). On the basis of lithological analysis and together with radiocarbon ages obtained from Core MD01-2425, the mass-wastings are initially governed by climatic and water level changes during the Late Pleistocene to Holocene (Eriş et al., 2012; Drab et al., 2015; Beck et al., 2015). On the basis of previous seismic and core studies in the SoM, the water level was well below the present shelf break (−110 m) during the lacustrine phase (Smith et al., 1995; Çağatay et al., 2003, 2009; Eriş et al., 2007, 2011; McHugh et al., 2008; Vidal et al., 2010). As a result of drawdown, the shelf areas of the Çınarcık Basin were introduced to a heavy erosion leading to increased sediment supply to the deep basin due to a relatively low trapping efficiency particularly on a narrow northern shelf of the basin. Accordingly, unstable sediments with a great thickness on the shelf margin and steep slopes of the basin would have been more susceptible to slope failure during the lacustrine phase of the SoM.

In Core MD01-2425 from the Çınarcık Basin, grain-size and magnetic susceptibility (MS) analyses together with the visual lithological description of the seismoturbidite layers indicates that a basin-wide event, involving multiple simultaneous underwater

slope failures, gave rise to deposition of the seismoturbidites (Eriş et al., 2012; Beck et al., 2015). The reason for amalgamated seismoturbidites can be explained that triggering by the main shock would lead to spontaneous surge flows, whereas after shock-triggered flows would be sequential. Some of amalgamated layers are compositionally distinct in coarse fraction from the underlying and overlying layers that suggests multiple slides from different sources. Another possible cause for amalgamated layers could be the reflected turbidites (Eriş et al., 2012). Based on the seismic and bathymetry data from the surrounding shelves of the Çınarcık Basin, the shelf break and upper slope areas of the basin have been the depositional sites for unstable sediments that could be remobilized by slumping during large earthquakes. Such failures may generally result from either increase in shear stress or a reduction in shear strength due to the generation of excess pore pressure within the sediments on slopes. Accordingly, increasing shear stress or generation of sufficient pore pressure so as to promote failure of the basin slopes have been attributed to sea level fall and/or seismic shaking in the SoM. The observations from the seismic and core data from various studies suggest a close connection between mass failure deposits and turbidites (Fig. 25; Eriş et al., 2012; Drab et al., 2015; Beck et al., 2015; McHugh et al., 2014). The lateral transition from slump/debris flow deposits into turbidites on the mud-dominated slopes of the SoM clearly demonstrates the transformation from slumping into debris flow then into turbidity current (Mulder et al., 1995). Slide on the upper slopes would have been transformed into non-cohesive debris-flows, most of which were confined within submarine canyons along the basin slopes. Such non-cohesive plastic flows may be then transformed into turbidity currents on the lower slope of the subbasins of the SoM.

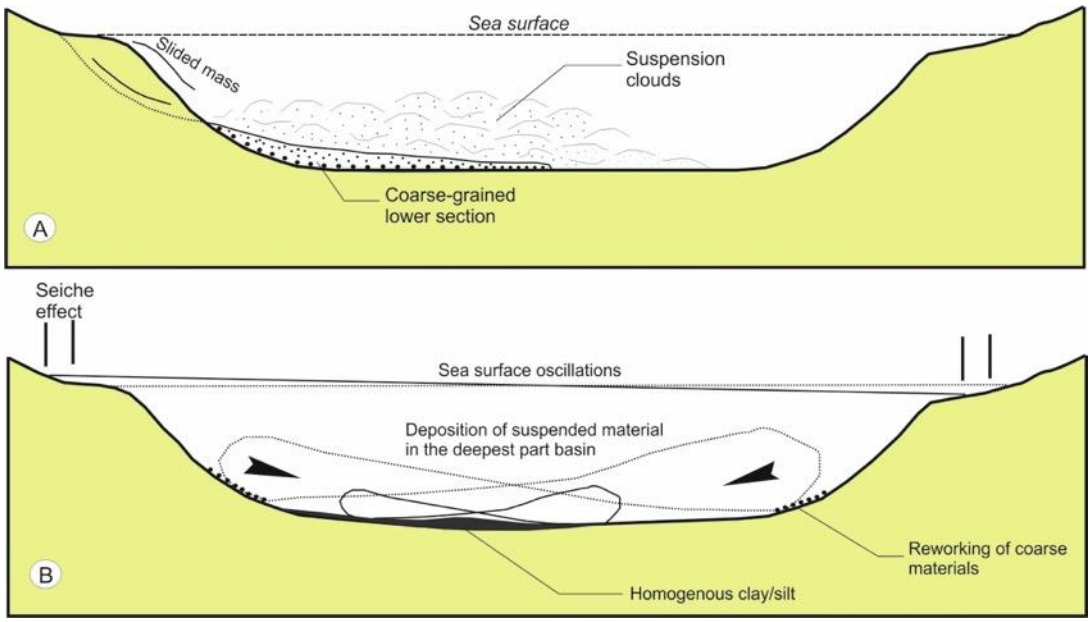

Figure 39. The hypothesis of depositional process of earthquake-triggered seismoturbidites in the deep basins of the SoM (Beck et al., 2007; Eriş et al., 2012).

As documented in many core studies, seismoturbidites sequence can be subdivided into two different parts with respect to lithologic compositions that presumably reflect different depositional processes regarding to various grain settling modes due to significant variations in sedimentation dynamics. For the coarse-grained lower part of the layer, the structureless, coarse-tail graded unit itself is more indicative of low shear stress during a period of rapid sediment fall-out as a traction carpet formed at the base of a turbulent suspension (Fig. 39). According to grain-size measurements on Core MD01-2425 from the Çınarcık Basin, the negatively skewed distribution of massive sandy part of the seismoturbidite layer is due to the excess of coarse sediment, and indicates the prevalence of high-energy conditions (Eriş et al., 2012). As the sandy part grades upward into clayey sand, the skewness increases towards positive values due to high volume of clay fractions. This can be explained as the turbidity current decelerated, more sediment settled out, the deposits became finer and more poorly sorted and tended toward positive skewness upwards. However, the combination of various modes of transport (rolling,

saltation and suspension) may eventually lead to poorly sorted sediments. However, poor sorting and co-deposition of sand and silt with clay have been proposed to be the most significant features of seismoturbidites (Shiki et al., 2000; Arnaud et al., 2002; Goldfinger et al., 2003; Schnellmann et al., 2005; Beck et al., 2007; Carrillo et al., 2008). On the other hand, the high clay content reflects another important feature of seismoturbidite layers in the core. The distinct boundary between the coarse grained basal part and the upper homogeneous clay and lack of clear internal structures differ from the usual configuration of classical turbidites (Cita et al., 1996; Shiki et al., 2000). Moreover, its greater thickness and absence of large clasts in this peculiar type of redeposited sediment are significant evidences to differ from debris flow (Cita et al., 1982).

Deposition of the homogeneous part of the seismoturbidite layers can be explained by a deep-seated separation of an upper fine-grained cloud from the coarse-grained lower part. The specific particle settling with a high segregation of fine-grained (suspended-load) from coarser (silt, sand) material implies a long lasting bottom current effect (Fig. 39). Such a suspension cloud was deposited with a short time lag after the sandy layer deposit and is regarded as a very fine-grained distal seismoturbidite layer. The study on the same core (MD01-2425) from the Çınarcık Basin by Beck et al. (2015) favor a hypothesis implying two combined mechanisms: (1) the water vertical density profile led to more hyperpycnal distribution of gravity reworked sediments, and (2) coarse material strongly decreased due to change in weathering condition.

References

Aksu, A.E., Hiscott, R.N., Yasar, D., 1999. Oscillating Quaternary water levels of the Marmara Sea and vigorous outflow into the Aegean Sea from the Marmara Sea Black Sea drainage corridor. Marine Geology 153 (1–4), 275–302.

Armijo, R., Pondard, N., Meyer, B., Mercier de Lepinay, B., Uçarkus, G., Malavieille, J., Dominguez, S., Gustcher, M.A., Beck, C., Çağatay, N., Çakir, Z., İmren, C., Kadir, E., Natalin, MARMARASCARPS cruise party, 2005. Submarine fault scarps in the Sea of Marmara pull-apart (North Anatolian Fault): implications for seismic hazard in Istanbul. Geochemistry, Geophysics, Geosystems 6, 1–29.

Arnaud, F., Lignier, V., Revel, M., Desmet, M., Beck, C., Pourchet, M., Charlet, F., Trentesaux, A., Tribovillard, N., 2002. Flood and earthquake disturbance of 210Pb geochronology (Lake Anterne, NW Alps). Terra Nova 14, 225–232.

Ambraseys, N.N., 2002a. The seismic activity in the Marmara Sea region over the last 2000 years. Bulletin of the Seismological Society of America 92, 1–18.

Ambraseys, N.N., 2009. Earthquakes in the Mediterranean and Middle East: A Multidisciplinary

Study of Seismicity up to 1900. Cambridge University Press, Cambridge, U. K. (947 pp.).

Avşar, U., 2013. Lacustrine paleoseismic records from the North Anatolian Fault, Turkey. PhD Thesis memoir, University of Ghent, 209 pp.

Beck, C., Manalt, F., Chapron, E., Van Rensbergen, P., De Batist, M., 1996. Enhanced seismicity in early post-glacial period: evidences from the posy-Würm sediments of Lake Annecy, northwestern

Alps, J. Geodynam., 22, 155–171.

Beck, C., Mercier de Lépinay, B., Schneider, J.-L., Cremer, M., Çağatay, N., Wendenbaum, E., Boutareaud, S., Ménot, G., Schmidt, S., Weber, O., Eris, K., Armijo, R., Meyer, B., Pondard, N., Gutscher, M.-A., and the MARMACORE Cruise Party, Turon, J.-L., Labeyrie, L., Cortijo, E., Gallet, Y., Bouquerel, H., Gorur, N., Gervais, A., Castera, M.-H., Londeix, L., de Rességuier, A., and Jaouen, A., 2007. Late Quaternary co-seismic sedimentation in the Sea of Marmara's deep basins, in: "Sedimentary Records of Catastrophic Events", edited by: Bourrouilh-Le Jan, F., Beck, C., and Gorsline, D., Spec. Iss, Sediment. Geol., 199, 65–89.

Beck, C., Reyss, J.-L., Leclerc, F., Moreno, E., Feuillet, N. and GWADASEIS Cruise Scientific Party: Barrier, L., Beauducel, F., Boudon, G., Clément, V., Deplus, C., Gallou, N., Lebrun, J.-F., Le Friant, A., Nercessian, A., Paterne, M., Saurel, J.-M., Pichot, T., Vidal, C., 2012. Identification of deep subaqueous co-seismic scarps through specific coeval sedimentation in Lesser Antilles: implication for seismic hazard. Natural Hazards and Earth System Sciences, Special Issue "Subaqueous Paleoseismology" (D. Pantosti Edt.), http://dx.doi.org/10.5194/nhess-12-1-2012, 1755–1767.

Beck, C., Campos C., Eriş, K. K., Çağatay, N., Mercier de Lepinay, B., and Jouanne, F., 2015. Estimation of successive coseismic vertical offsets using coeval sedimentary events–application to the southwestern limit of the Sea of Marmara's Central Basin (North Anatolian Fault). Nat. Hazards Earth Syst. Sci., 15, 247–259.

Campos, C., Beck, C. Crouzet, C., Demory, F., VanWelden, A., and Eris, K., 2013. Deciphering hemipelagites from homogenites through Magnetic Susceptibility Anisotropy. Paleoseismic implications (Sea of Marmara and Gulf of Corinth), Sediment. Geol., 292, 1–14.

Carrillo, E., Beck, C., Audemard, F.A., Moreno, E., Ollarves, R., 2008. Disentangling Late Quaternary climatic and seismo-tectonic controls on Lake Mucubaji sedimentation (Merida Andes, Venezuela). Palaeogeography Palaeoclimatology Palaeoecology 259, 284–300.

Chapron, E., Beck, C., Pourchet, M., and Deconinck, J.-F., 1999. 1822 earthquake-triggered homogenite in Lake Le Bourget (NW Alps), Terra Nova, 11, 86–92.

Cita, M.B., Rimoldi, B., 1997. Geological and geophysical evidence for a Holocene tsunami deposit in the eastern Mediterranean deep-sea record. In:Hancock, P.L., Michetti, A.M., et al. (Eds.), Paleoseismology; understanding past earthquakes using Quaternary geology. : Journal of Geodynamics, 24. 1–4, pp. 293–304.

Cita, M.B., Aloisi, G., 2000. Deep-sea tsunami deposits triggered by the explosion of Santorini (350 y BP), Eastern Mediterranean. Sedimentary Geology 135, 181–203.

Çagatay, M., N. Görür, O. Algan, C. Eastoe, A. Tchapalyga, D. Ongan, T. Kuhn, and I. Kuscu., 2000. Late Glacial–Holocene palaeoceanography of the Sea of Marmara: Timing of connections with the Mediterranean and the Black Seas, Mar. Geol. 167, nos. 3/4, 191–206.

Cormier, M.-H., Seeber, L., McHugh, C.M.G., Polonia, A., Çağatay, M.N., Emre, Ö., Gasperini, L., Görür, N., Bertoluzzi, G., Bonatti, E., Ryan,W.B.F., Newman, K.R., 2006. The North Anatolian fault in the Gulf of Izmit (Turkey): rapid vertical motion in response to minor bends of a non-vertical continental transform. J. Geophys. Res. 111, B04102. doi:10.1029/2005JB003633.

Çağatay, M. N., Eriş, K., Ryan, W. B. F., Sancar, Ü., Polonia, A., Akçer, S., Biltekin, D., Gasperini, L., Görür, N., Lericolais, G., and Bard, E., 2009. Late Pleistocene–

Holocene evolution of the northern shelf of the Sea of Marmara, Mar. Geol., 265, 87–100, 2009.

Çağatay, N., Erel, L., Bellucci, L. G., Polonia, A., Gasperini, L., Eriş, K. K., Sancar, Ü., Biltekin, D., Uçarkuş, G., Ulgen, Ü. B., and Damci, E., 2012. Sedimentary earthquake records in the Izmit Gulf, Sea of Marmara, Turkey, Sediment. Geol., 282, 347–359.

Drab, L., Hubert Ferrari, A., Schmidt, S., and Martinez, P., 2012. The earthquake sedimentary record in the western part of the Sea of Marmara, Turkey, Nat. Hazards Earth Syst. Sci., 12, 1235–1254, doi:10.5194/nhess-12-1235-2012, 2012.

Drab, L., J. Carlut, A. Hubert-Ferrari, P. Martinez, G. LePoint, and M. El Ouahabi., 2015. Paleomagnetic and geochemical record from cores from the Sea of Marmara, Turkey: Age constraints and implications of sapropelic deposition on early diagenesis, Marine Geology 360, 40–54, 0025-3227, doi: 10.1016/j.margeo.2014.12.002.

Eriş, K.K., Ryan, W.B.F., Çağatay, M.N., Sancar, U., Lericolais, G., Ménot, G., Bard, E., 2007. The timing and evolution of the post-glacial transgression across the Sea of Marmara shelf south of İstanbul. Marine Geology 243, 57–76.

Eriş, K.K., Çağatay, N., Akçer, S., Gaperini, L., Mart, Y., 2011. Late glacial to Holocene sealevel changes in the Sea of Marmara: new evidence from high-resolution seismics and core studies. Geo-Marine Letters 31, 1–18.

Eriş, K., Çagatay, N. Beck, C., Mercier de Lepinay, B., and Campos, C., 2012. Late-Pleistocene to Holocene sedimentary fills of the Çınarcık Basin of the Sea of Marmara, Sediment. Geol., 281, 151–165.

Gasperini, L., Polonia, A., Çağatay, M.N., Bortoluzzi, G., ve Ferrante, V., 2011. Geological slip rates along the North Anatolian Fault in the Marmara region. Tectonics 30, TC6001.

Goldfinger, C., Nelson, C.H., Johnson, J.E., 2003. Holocene earthquake records from the Cascadia subduction zone and northern San Andreas fault based on precise dating of offshore turbidites. Annual Review of Earth and Planetary Sciences 31, 555–557.

Goldfinger, C., Morey, A.E., Nelson, C.H., Gutierrez-Pastor, J., Johnson, J.E., Karabanov, E., Chaytor, J., Eriksson, A., Shipboard Scientific Party, 2007. Rupture lengths and temporal history of significant earthquakes on the offshore and north coast segments of the Northern San Andreas Fault based on turbidite stratigraphy. Earth and Planetary Science Letters 254, 9–27.

Goldfinger, C., C. H. Nelson, A. E. Morey, J. E. Johnson, J. R. Patton, E. Karabanov, J. Gutierrez-Pastor, A. T. Eriksson, E. Gràcia, G. Dunhill., 2012. Turbidite event history: Methods and implications for Holocene paleoseismicity of the Cascadia subduction zone, U.S. Geol. Surv. Prof. Paper 1661–F, 170 pp.

Görür, N., Çağatay,M.N., 2010. Geohazards rooted from the northern margin of the Sea of Marmara since the late Pleistocene: a review of recent results. Natural Hazards 54, 583–603.

Grácia, E., Vizcaino, A., Escutia, C., Asioli, A., Rodes, A., Pallas, R., Garcia-Orellana, J., Lebreiro, S., Goldfinger, C., 2010. Holocene earhquake record offshore Portugal (SW Iberia): testing turbidite paleoseismology in a slow-convergence margin. Quaternary Science Reviews 29, 1156–1172.

Grall C, Henry P, Tezcan D., 2012. Heat flow in the Sea of Marmara Central Basin: possible implications for the tectonic evolution of the North Anatolian fault. Geology 40: 3–6.

Grall, C., Herny, P., Thomas, Y., Westbrook, G.K., Çağatay, M.N., Marsset, B., Saritas, H., Çifici, G., Geli, L., 2013. Slip rate estimations along the western segment of the

Main Marmara Fault over the last 405–490 ka by correlating mas transport deposits. Tectonics 32, 1–15.

Hiscott, R.N., Aksu, A.E., Yaşar, D., Kaminski, M.A., Mudie, P.J., Kostylev, V.E., MacDonald, J.C., Isler, F.I., Lord, A.R., 2002. Deltas south of the Bosphorus Strait record persistent Black Sea outflow to the Marmara Sea since ~10 ka. Mar. Geol. 190, 95–118.

Honkura, Y, Isikara, A.M., 1991. Multidisciplinary research on fault activity in the western part of the North Anatolian Fault Zone. Tectonophysics 193, 347-357.

Lorenzoni, L., Benitez-Nelson, C. R., Thunell, R. C., Hollander, D., Varelan, R., Astor, Y.,Audemard, F. A., and Muller-Karger, F. E., 2012. Potential role of event-driven sediment transport on sediment accumulation in the Cariaco Basin, Venezuela, Mar. Geol., 105–110, doi:10.1016/j.margeo.2011.12.009.

Schnellmann, M., Flavio, S.A., Domenico, G., Judith, A.M., 2005. Mass movementinduced fold-and-thrust belt structures in unconsolidated sediments in Lake Lucerne (Switzerland). Sedimentology 52, 271–289.

McHugh, C., Seeber, L., Cormier, M.H., Dutton, J., Çağatay, N., Polonia, A., Ryan, W.B.F., Görür, N., 2006. Submarine earthquake geology along the North Anatolian Fault in the Marmara Sea, Turkey: a model for transform basin sedimentation. Earth and Planetary Science Letters 248, 661–684.

McHugh, C., Seeber, L., Braudy, N., Cormier, M.-H., Davis, M. B., Diebold, J. B., Dieudonne, N., Douilly, R., Gulick, S. P. S., Hornbach, M. J., Johnson, H. E. III, Ryan Miskin, K., Sorlien, C., Steckler, M., Symithe, S. J., and Templeton, J., 2011. Offshore sedimentary effects of the 12 January 2010 Haiti earthquake, Geology, 39, 723–726, doi:10.1130/G31815.1.

McHugh, C., Braudy, N.M., Çağatay, N., Sorlien, C., Cormier, M.-H., Seeber, L., and Henry, P., 2014 Sea floor fault ruptures along the North Anatolia Faultin the Marmara Sea, Turkey: Link with the adjacent basin turbidite record, Mar. Geol., 353, 65–83.

McClusky, C.M.G., Reilinger, R., Mahmoud, S., Ben Sari, D., Tealeb, A., 2003. GPS constraints

on Africa (Nubia) and Arabia plate motions. Geophysical Journal International 155, 126–138.

Moernaut, J., 2011. Sublacustrine landslide processes and their paleoseismological significance: revealing the recurrence rate of giant earthquakes in South-Central Chile, PhD Thesis, University of Ghent, 274 pp.

Moretti, I., Lykousis, V., Sakellariou, D., Reynaud, J.-Y., Benziane, B., Prinzhoffer, A., 2004. Sedimentation and subsidence rate in the Gulf of Corinth: what we learn from the Marion-Dufresne's long-piston coring. Comptes-Rendus Géosciences 336 (4/5), 291–299.

Mulder, T., Syvitski, J.P.M., 1995. Turbidity currents generated at river mouths during exceptional discharges to the world oceans. Journal of Geology 103, 285–299.

Mulder, T., Alexander, J., 2001. The physical character of subaqueous sedimentary density currents and their deposits. Sedimentology 48, 269–299.

Murru M., Akinci A., Falcone G. Pucci S., Console R. Parson T., 2016. M≥7 Earthquake Rupture Forecast and Time-Dependent Probability for the Sea of Marmara Region, Turkey, J. Geophys. Res. Solid Earth, 121, doi:10.1002/2015JB012595.

Nakajima, T., Kanai, Y., 2000. Sedimentary features of seismoturbidites triggered by the 1983 and older historical earthquakes in the eastern margin of the Japan Sea. Sedimentary Geology 135, 1–19.

Nemec, W., 1990. Aspect of sediment movement on step delta slope. In: Colella, A., Prior, D.B. (Eds.), Coarse Grained Deltas. International Association of Sedimentologists Special Publication, 10. Blackwell, Oxford, pp. 29–74.

Özeren, M.S., Çağatay, M.N., Postacıoğlu, N., Şengör, A.M.C., Görür, N., Eriş, K., 2010. Mathematical modelling of a potential tsunami associated with a late glacial submarine landslide in the Sea of Marmara. Geo-Marine Letters 30, 523–539.

Polonia, A., Gasperini, L., Amorosi, A., Bonatti, E., Bortoluzzi, G., Çağatay, N., Capotondi, L., Cormier,M.-H., Görür, N., McHugh, C., Seeber, L., 2004. Holocene slip rate of the North Anatolian Fault beneath the Sea of Marmara. Earth Planet. Sci. Lett. 227, 411–426.

Postma, G., Babic, L., Zupanic, J., Roe, S.L., 1988. Delta-front failure and associated bottomset deformation in a marine, gravelly Gilbert-type delta. In: Nemec, N., Steel, R.J. (Eds.), Fan Deltas: Sedimentology and Tectonic Settings. Blackie, Glasgow & London, pp. 91–102.

Piper, D. J. W., Cochonat, P., Ollier, G., Le Drezen, E., Morrison, M., and Baltzer, A., 1992. Evolution progressive d'un glissement rotationnel en un courant de turbidité : cas du séisme de 1929 des Grands Bancs (Terre Neuve), Comptes-Rendus de l'Académie des Sciences, Paris, 314, 1057–1064.

Pouderoux, H., Lamarche, G., Proust, J.-N., 2012. Building a 18,000 year-long paleoearthquake record from detailed deep-sea turbidite characterization in Poverty Bay, New Zealand. Natural Hazards and Earth System Sciences 12, 2077–2101.

Prior, D.B., Suhayda, J.N., Lu, N.Z., Bornhold, B.D., Keller, G.H., Wiseman, W.J., Wright, L.D., Yang, Z.S., 1989. Storm wave reactivation of a submarine landslide. Nature 341, 47–50.

Sarı, E., Çağatay, M.N., 2006. Turbidites and their association with past earthquakes in the deep Çınarcık Basin of the Marmara Sea. Geo-Marine Letters 26, 69–76.

Schnellmann, M., Flavio, S.A., Domenico, G., Judith, A.M., 2005. Mass movementinduced fold-and-thrust belt structures in unconsolidated sediments in Lake Lucerne (Switzerland). Sedimentology 52, 271–289.

Shiki, T., Kumon, F., Inouchi, Y., Kontani, Y., Sakamoto, T., Tateishi, M., Matsubara, H., Fukuyama, K., 2000. Sedimentary features of the seismo-turbidities, Lake Biwa, Japan. Sedimentary Geology 135, 37–50.

Siegenthaler, C., Finger, W., Kelts, K., and Wang, S., 1987. Earthquake and seiche deposits in Lake Lucerne, Switzerland, Eclogae Geolog. Helvetiae, 80, 241–260.

Smith, A.D., Taymaz, T., Oktay, F., Yüce, H., Alpar, B., Başaran, H., Jackson, J.A., Kara, S., Şimşek, M., 1995. High resolution seismic reflection profiling in the Sea of Marmara (northwest Turkey): late Quaternary sedimentation and sea-level changes. Bulletin of the Geological Society of America 107, 923–936.

Strasser, M., Anselmetti, F. S., Fäh, D., Giardini, D., and Schnellmann, M., 2006. Magnitudes and source areas of large prehistoric northern Alpine earthquakes revealed by slope failures in lakes, Geology, 34, 1005–1008.

St-Onge, G., Chapron, E.,Mulsow, S., Salas,M., Viel,M., Debret, M., Foucher, A.,Mulder, Th., Winiarski, Th., Desmet,M., Costa, P.J.M., Ghaleb, B., Jaouen, A., Locat, J., 2012. Comparison of earthquake-triggered turbidites from the Saguenay (Eastern Canada) and Reloncavi (Chilean margin) Fjords: implications for paleoseismicity and sedimentology. Sedimentary Geology 243–244, 9–107.

Thunell, R., Tappa, E., Valera, R., Llano, M., Astor, Y., Muller-Karger, F., Bohrer, R., 1999. Increased marine sediment suspension and fluxes following an earthquake. Nature 398, 233–236.

Vidal, L., Ménot, G., Joly, C., Bruneton, H., Rostek, F., Çağatay, M.N., Major, M., Bard, E., 2010. Hydrology in the Sea of Marmara during the last 23 ka: implications for timing of Black Sea connections and sapropel deposition. Paleoceanography 25 (1), pa1205. http://dx.doi.org/10.1029/2009pa001735.

Wells, D.L., Coppersmith, K.J., 1994. New empirical relationships among magnitude, rupture length, rupture width, rupture area, and surface displacement. Bulletin of the Seismological Society of America 84, 974–1002.

Wetzler, N., Marco, S., and Heifetz, E., 2010. Quantitative analysis of shear-induced turbulence in lake sediments, Geology, 38, 303–306, 2010.

Zitter TAC, Grall C, Henry P., Özeren, M.S., Çağatay, M.N., Şengör, A.M.C., Gasperini, L., Mercier de Lépinay, B. Géli, L., 2012. Distribution, morphology and triggers of submarine mass wasting in the Sea of Marmara. Mar Geol 329:58–74.